MODELLING 2-LAYER ROTATING FLOWS

J. W. KING

NUMERICAL ANALYSIS REPORT 7/81

The author would like to acknowledge financial support from the Meteorological Office and the SERC.

CONTENTS

1. INTRODUCTION

In Geophysical Fluid Dynamics an important and much studied phenomenon is that of baroclinic instability. When a fluid is baroclinically unstable, small waves will grow to a finite amplitude: in a meteorological context the waves observed in the midlatitude Westerlies of the Earth's atmosphere, and the meanders observed in many ocean currents are believed to be baroclinic waves (e.g. Lorenz 1967, Gill et al. 1974). Similar observations have been made in two simple experiments (see reviews by Hide and Mason 1975, Hart 1972). Because of their key role in the dynamics of many geophysical systems, a detailed understanding of the behaviour of these baroclinic disturbances is essential. Models for idealised atmospheric flows have been examined using numerical techniques (Hoskins and Simmons 1976, 1977), but it is not straightforward to test these results against observation. The main aim of the present work is to develop a numerical model of one of the two experiments, the two-layer system, where such comparisons should be simpler.

A fluid is said to be baroclinically unstable when it possesses gravitational potential energy available for transformation into kinetic energy; i.e. when the density gradient and the gravitational force are not parallel ($\underline{g} \times \nabla\rho \neq \underline{0}$) . Such a situation is shown in Fig.1.

If a disturbance could interchange the two fluid particles situated at A and B , then the change in potential energy, ΔPE is given by

$$\begin{aligned} \Delta PE &= \Delta PE_{A\to B} + \Delta PE_{B\to A} \\ &= \rho\, g\, \delta h - (\rho + \delta\rho)\, g\, \delta h \\ &= -\, g\, \delta\rho\, \delta h \\ &< 0 \quad . \end{aligned}$$

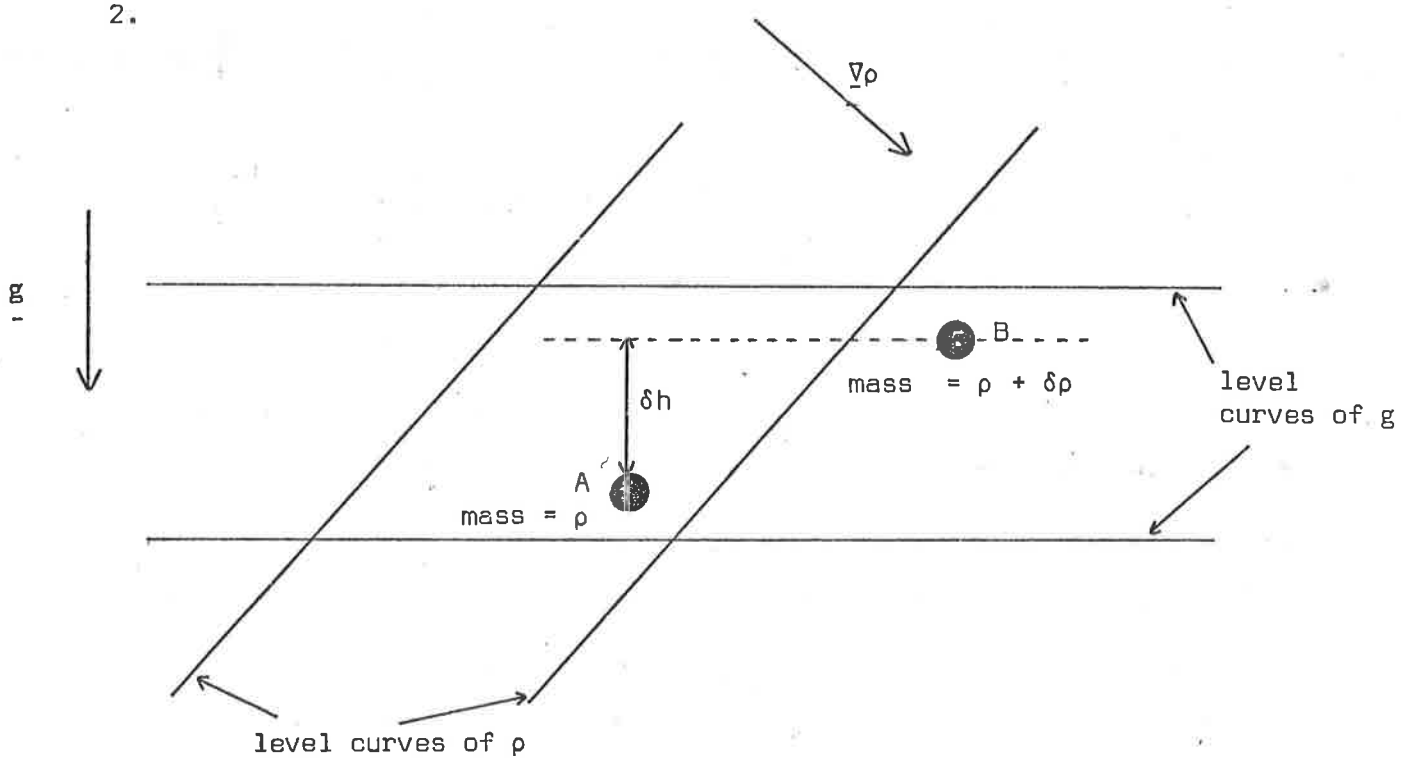

Fig.1 :The baroclinic instability of fluid elements at A and B

Hence a disturbance of the correct form will convert potential energy, called the available potential energy, into kinetic energy, and the disturbance can grow in amplitude. This idea is similar to that employed in the analysis of instability of Couette flow, and many other hydrodynamic stability phenomena.

In atmospheric flows the rotation of the Earth and Solar heating provide the source of potential energy. In the first of the two laboratory experiments which model baroclinic instability, the thermal annulus experiment, the mechanism of potential energy generation is similar to that for atmospheric flows. The apparatus consists of an annulus filled with a single fluid subjected to a lateral temperature gradient. The temperature gradient is induced by heating and cooling the inner and outer (or outer and inner) walls of the annulus respectively. This is shown in Fig.2. With the whole

apparatus rotating rapidly various kinds of regular and irregular, periodic and aperiodic motions have been recorded (e.g. Hide 1969): some of these are shown in Fig.3.

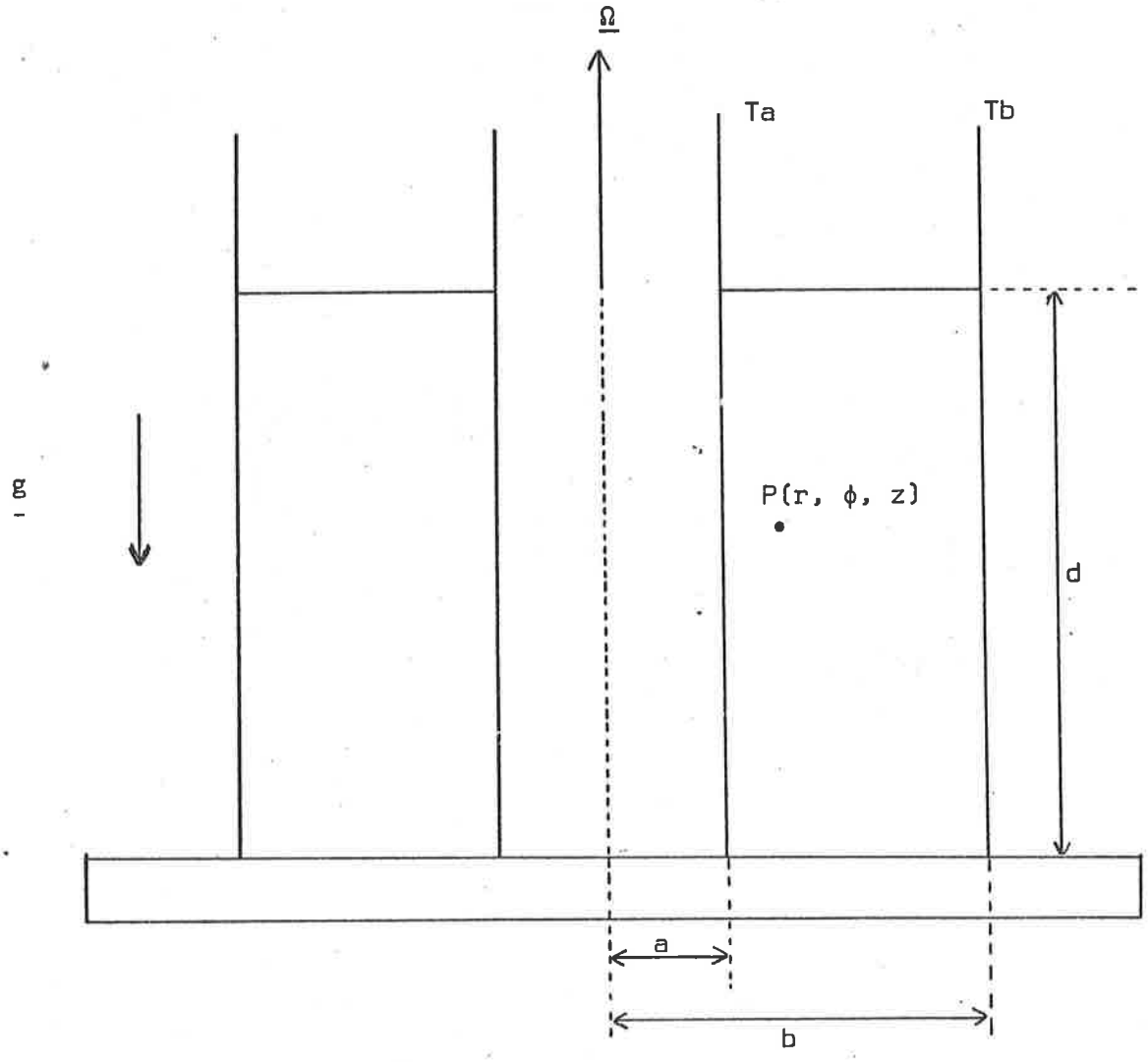

Fig. 2 : Schematic diagram of a rotating annulus subject to a horizontal temperature gradient. $\underline{g} = (0, 0, -g)$ is typically $>> \Omega^2 r$ and the temperature gradient is maintained by temperature baths at r = a and r = b.

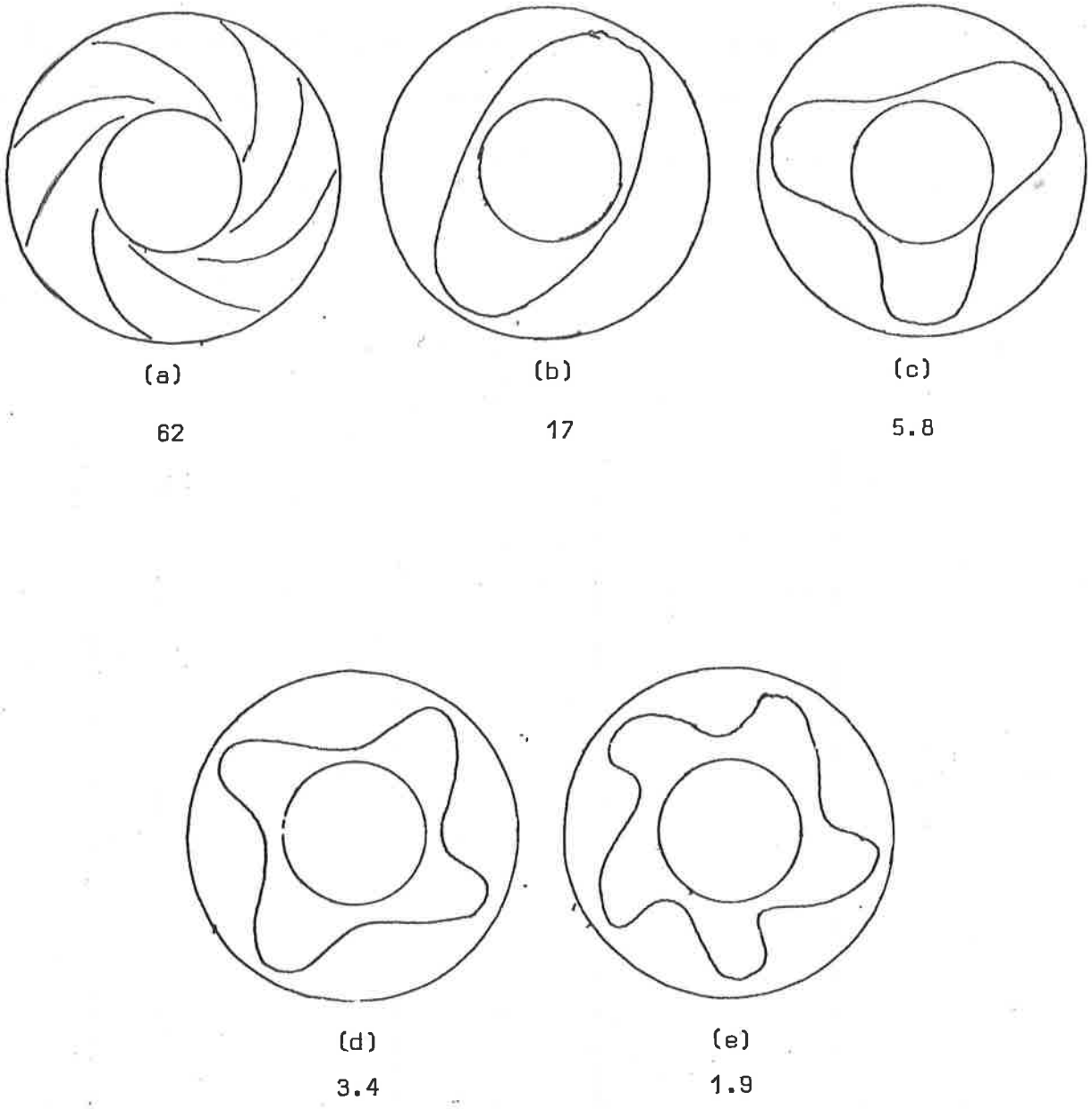

Fig. 3 : Top surface flow patterns at different values of X, where X is related to the temperature gradient and rotation rate. (a) depicts axisymmetric flow at a slow rotation, while (b) - (e) depict typical wave motions at progressively faster rotations.

The other laboratory experiment, the two-layer system, consists of a similar annulus, this time filled with two liquids which are gravitationally stable when the annulus is stationary. When the annulus is rotating a mechanical driving force applied through the lid generates the conditions for baroclinic instability, and motions, similar to those for the heated annulus experiment, are observed. The laboratory system is described in more detail and mathematical and numerical models for it are derived in Section 2.

The typical evolution of a small disturbance is as follows: for as long as the perturbations to some equilibrium solution are small they will grow exponentially; however, when their amplitudes become large enough so that non-linear interactions become significant a balance between the conversion of potential energy to kinetic energy and the removal of kinetic energy by dissipative mechanisms will develop, and finite amplitude baroclinic waves are observed. It is the behaviour of such finite amplitude waves in the two-layer system that is the subject of the present study: for while an extensive literature exists on the initial growth of infinitesimal disturbances (see, for example, Hide 1969), the analysis of finite amplitude waves is much less tractable and only a few limited analyses have been carried out (Drazin 1970, Pedlosky 1970, 1971, Smith 1977). Indeed, one of the main characteristics of all finite-amplitude analyses is that they are only weakly-nonlinear, and for a highly idealised number of wave modes. With a numerical model we will be in a position to analyse strongly-nonlinear parameter regimes, and to verify some of the weakly-nonlinear analysis.

In this report we present a verification of the numerical model that has been developed: linear analyses of the mathematical and numerical models are presented in Sections 3 and 4, with a detailed comparison of

these in section 5. Some nonlinear comparisons are made in Section 6, and in the last section we are able to indicate our conclusions about the model and to assess the areas in which our model will be of particular use.

2. MATHEMATICAL FORMULATION AND NUMERICAL APPROXIMATION

2.1 The Model and Formulation of the Equations

The experimental model in Dr. Hide's laboratory at the Meteorological Office in Bracknell consists of two layers of homogeneous fluid, each with a constant (but different) density, contained in an annulus which is free to rotate about its vertical axis. The lighter fluid lies above the denser so that the system is gravitationally stable when stationary. There is a lid in contact with the upper surface of the lighter fluid, which is free to rotate, independently of the annulus, about its axis. Hence, when the annulus and lid are rotating with constant but different angular velocities, a baroclinically unstable interface is created between the two fluids and baroclinic waves will be observed. The apparatus is shown in Fig.4.

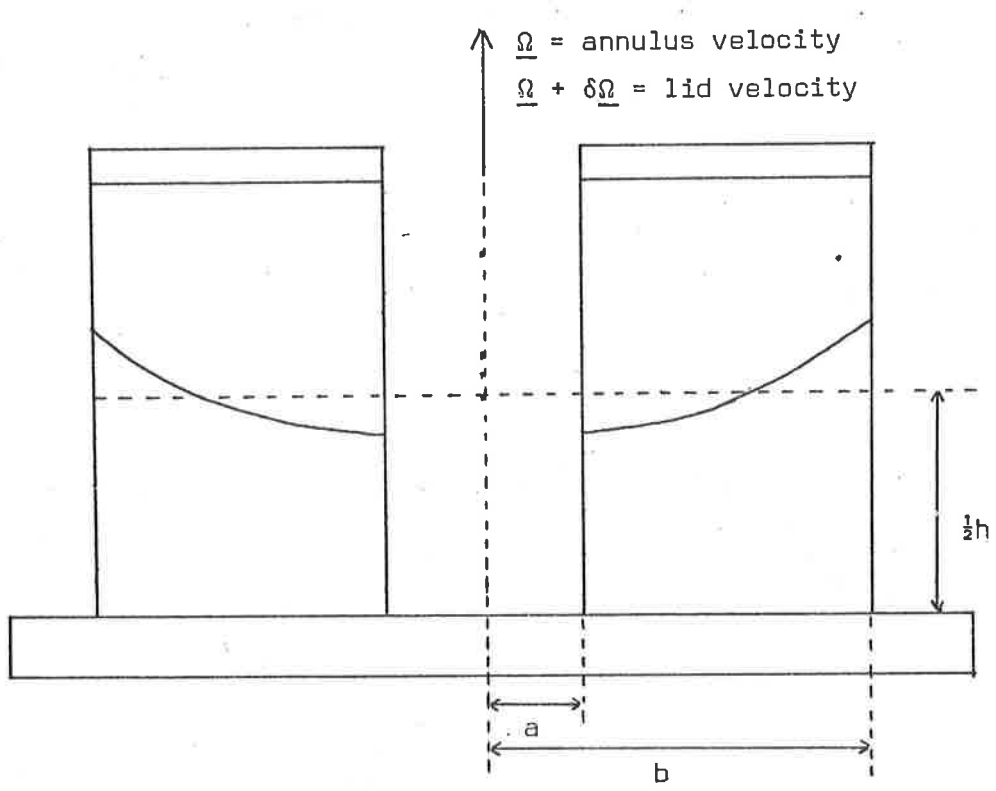

Fig. 4 : The two-layer system. A typical configuration of the interface is shown near $z = \frac{1}{2}h$.

For the mathematical formulation we shall follow Phillips (1954) and Pedlosky (1970) in modelling a long straight channel. Pedlosky has presented a detailed analysis of such a straight channel model (Pedlosky 1970, 1971, 1972) and it is really to facilitate this analysis that the cylindrical effects are neglected. We wish to compare our numerical results with this analysis: therefore we derive the model as follows.

The two fluids are contained within the planes given by $y' = 0$ and L, $z' = 0$ and D, where the dashes indicate dimensional quantities. The pressure in each layer is p_1' and p_2', the subscript 1 denoting the upper layer; the densities and velocities are given by ρ_n and $\underline{u}_n' = (u_n', v_n', w_n')$, for $n = 1$ and 2, respectively. This is shown in Fig.5.

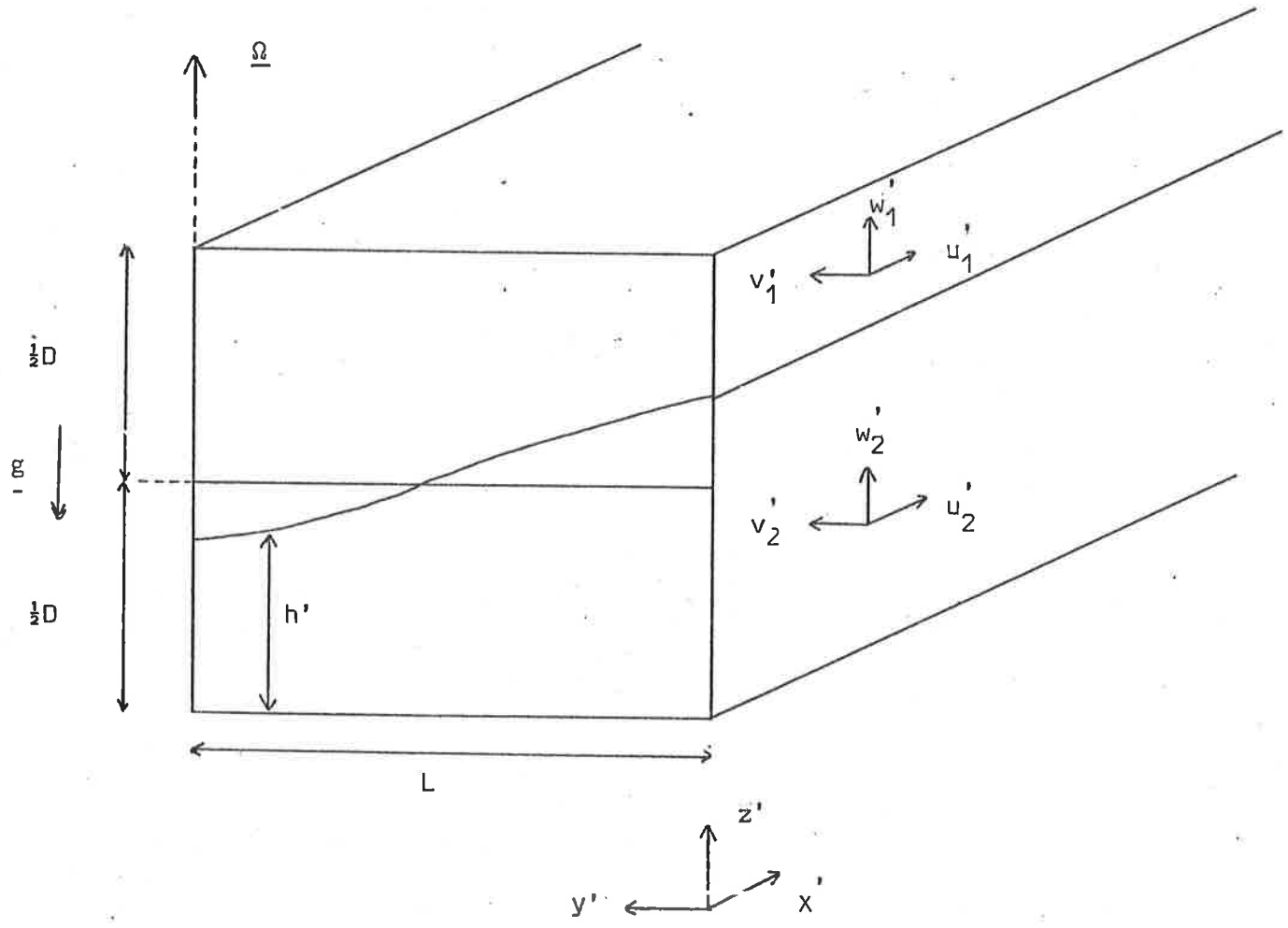

Fig. 5 : The two-layer straight channel model.

Non-dimensional variables are introduced using the following scalings:

$$
\left.
\begin{aligned}
(x,\ y) &= (x',\ y')/L \\
z &= z'/D \\
(u_n,\ v_n) &= (u_n',\ v_n')/U \\
w_n &= w_n' L/(UD) \\
t &= Ut'/L \\
p_1 &= [p'_1 + \rho_1 g(z' - D)]/(\rho_1 U f_o L) \\
p_2 &= [p_2' + \rho_2 g(z' - D/2 - \rho_1 gD/2)]/(\rho_2 U f_o L) \\
h &= (h' - D/2)/[\rho_1 U f_o L/g(\rho_2 - \rho_1)]
\end{aligned}
\right\} \qquad (2.1)
$$

where U is a characteristic scale for the horizontal velocity and where $2\Omega = f_o + \beta' y'$. Here the term $\beta' y'$ allows the rotation rate to vary linearly with y' thereby including, in a meteorological context, the effects of the earth's sphericity and, in a laboratory context, the effects of sloping end walls. If the model has sloping end walls then the top and bottom of the channel are not horizontal but are inclined at some small angle θ . (See Fig.6.)

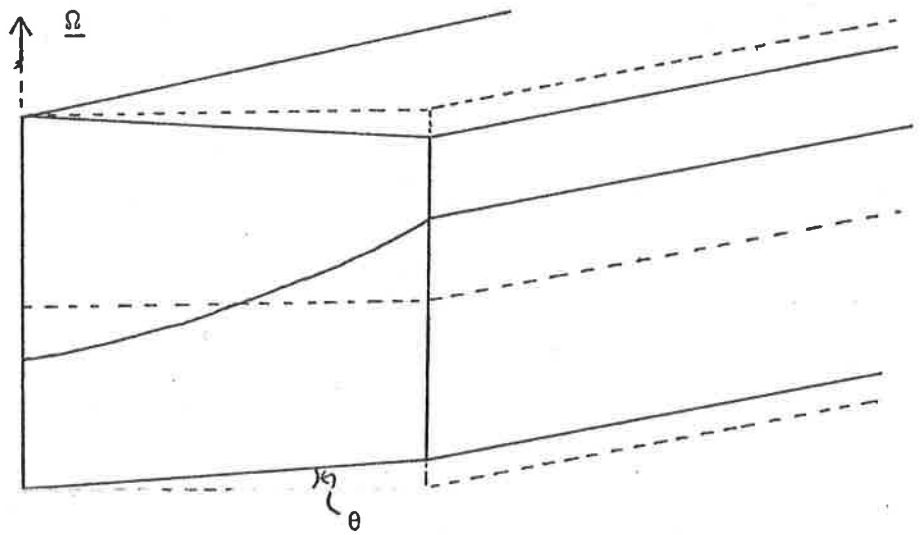

Fig. 6 : Sloping end walls in the two-layer system.

In a meteorological context, therefore, y' would be the northward pointing coordinate on the β-plane and x' would point east.

Defining

$$\left.\begin{aligned}
\varepsilon &= U/f_o L && \text{, the Rossby number}\\
E &= 2\nu/f_o D^2 && \text{, the Ekman number}\\
\beta &= \beta' L^2/U && \text{, the planetary vorticity factor}\\
\Delta\rho/\rho &= (\rho_2 - \rho_1)/\rho_2 && \text{, the density ratio}\\
F &= f_o^2 L^2 / \left[\frac{\Delta\rho}{\rho}\, g\, \frac{D}{2}\right] && \text{, the Froude number}\\
\delta &= D/L && \text{, the aspect ratio}
\end{aligned}\right\} \quad (2.2)$$

where these are all non-dimensional parameters, the Navier-Stokes equations in non-dimensional form are:

$$\left.\begin{aligned}
\varepsilon \frac{Du_n}{Dt} - (1 + \varepsilon\beta y)v_n &= -\frac{\partial p_n}{\partial x} + \frac{E}{2}\left(\delta^2\nabla^2 u_n + \frac{\partial^2}{\partial z^2} u_n\right)\\
\varepsilon \frac{Dv_n}{Dt} + (1 + \varepsilon\beta y)u_n &= -\frac{\partial p_n}{\partial y} + \frac{E}{2}\left(\delta^2\nabla^2 v_n + \frac{\partial^2}{\partial z^2} v_n\right)\\
\delta^2\varepsilon \frac{Dw_n}{Dt} &= -\frac{\partial p_n}{\partial z} + \delta^2 \frac{E}{2}\left(\delta^2\nabla^2 w_n + \frac{\partial^2}{\partial z^2} w_n\right)
\end{aligned}\right\} \quad \text{for } n = 1 \text{ and } 2, \quad (2.3)$$

where the continuity equation is,

$$\frac{\partial u_n}{\partial x} + \frac{\partial v_n}{\partial y} + \frac{\partial w_n}{\partial z} = 0 \qquad \text{for } n = 1 \text{ and } 2 ,$$

and

$$\nabla^2 \equiv \frac{\partial^2}{\partial x^2} + \frac{\partial^2}{\partial y^2} .$$

The kinematic boundary condition at the interface is

$$\varepsilon \frac{F}{2} \left\{ \frac{\partial h}{\partial t} + u_n \frac{\partial h}{\partial x} + v_n \frac{\partial h}{\partial y} \right\} = w_n \quad \text{at} \quad z = \tfrac{1}{2}(1 + \varepsilon F h) \ .$$

The parameters ε, E, $\Delta\rho/\rho$ and δ are assumed to be small compared with unity while F and β are taken to be $O(1)$. When the annulus or channel is rotating rapidly E and ε, being proportional to Ω^{-1}, are indeed small and this is not an unreasonable assumption. Typical laboratory values of these quantities are $\varepsilon = .1$, $E^{\frac{1}{2}} = .005$, $\Delta\rho/\rho = <<1$, $\delta = \frac{1}{2}$, $F = 7$ and $\beta = 1$.

We assume $E = o(\varepsilon^2)$, and make an expansion of the dependent parameters in powers of ε,

$$\underline{u}_n = \underline{u}_n^{(0)} + \varepsilon \underline{u}_n^{(1)} + \varepsilon^2 \underline{u}_n^{(2)} + \ldots$$

$$h = h^{(0)} + \varepsilon h^{(1)} + \varepsilon^2 h^{(2)} + \ldots$$

$$p_n = p_n^{(0)} + \varepsilon p_n^{(1)} + \varepsilon^2 p_n^{(2)} + \ldots \ ,$$

from which it follows, after substitution in (2.3) that to $O(1)$:

$$u_n^{(0)} = - \frac{\partial p_n^{(0)}}{\partial y}$$

$$v_n^{(0)} = \frac{\partial p_n^{(0)}}{\partial x}$$

$$0 = \frac{\partial p_n^{(0)}}{\partial z} \ .$$

Thus $\dfrac{\partial u_n^{(0)}}{\partial x} + \dfrac{\partial v_n^{(0)}}{\partial y} = 0$, and since $\dfrac{\partial w_n^{(0)}}{\partial z} = 0$, $w_n^{(0)} = 0$.

That is, for $\varepsilon << 1$, the lowest order motion is hydrostatic and geostrophic (i.e. independent of z) , $p_n^{(0)}$ being the geostrophic stream function, hereafter denoted by ψ_n .

Similarly, to $O(\varepsilon)$ we have:

$$\frac{\partial u_n^{(0)}}{\partial t} + u_n^{(0)} \frac{\partial u_n^{(0)}}{\partial x} + v_n^{(0)} \frac{\partial u_n^{(0)}}{\partial y} - v_n^{(1)} - \beta y v_n^{(0)} = - \frac{\partial p_n^{(1)}}{\partial x}$$

$$\frac{\partial v_n^{(0)}}{\partial t} + u_n^{(0)} \frac{\partial v_n^{(0)}}{\partial x} + v_n^{(0)} \frac{\partial v_n^{(0)}}{\partial y} + u_n^{(1)} + \beta y u_n^{(0)} = - \frac{\partial p_n^{(1)}}{\partial y}$$

$$0 = \frac{\partial p_n^{(1)}}{\partial z}$$

$$\frac{\partial u_n^{(1)}}{\partial x} + \frac{\partial v_n^{(1)}}{\partial y} + \frac{\partial w_n^{(1)}}{\partial z} = 0$$

$$\frac{F}{2} \left[\frac{\partial h^{(0)}}{\partial t} + u_n^{(0)} \frac{\partial h^{(0)}}{\partial x} + v_n^{(0)} \frac{\partial h^{(0)}}{\partial y} \right] = w_n^{(1)} .$$

Eliminating $p_n^{(1)}$ between the first two of these equations yields

$$\frac{\partial \zeta_n^{(0)}}{\partial t} + u_n^{(0)} \frac{\partial \zeta_n^{(0)}}{\partial x} + v_n^{(0)} \frac{\partial \zeta_n^{(0)}}{\partial y} + \beta v_n^{(0)} = \frac{\partial w_n^{(1)}}{\partial z} \qquad (2.4)$$

where $\zeta_n^{(0)} = \nabla^2 \psi_n = \frac{\partial v_n^{(0)}}{\partial x} - \frac{\partial u_n^{(0)}}{\partial y}$.

Since the velocities in each layer are independent of z to first order, we may integrate (2.4) across each layer. Using the kinematic boundary condition we find:

$$\left[\frac{\partial}{\partial t} + u_1^{(0)} \frac{\partial}{\partial x} + v_1^{(0)} \frac{\partial}{\partial y} \right] \left[\zeta_1^{(0)} + F h^{(0)} \right] + \beta v_1^{(0)} = 2 w_1^{(1)} \quad (x, y, 1)$$

$$\left[\frac{\partial}{\partial t} + u_2^{(0)} \frac{\partial}{\partial x} + v_2^{(0)} \frac{\partial}{\partial y} \right] \left[\zeta_2^{(0)} - F h^{(0)} \right] + \beta v_2^{(0)} = - 2 w_2^{(1)} \quad (x, y, 0) \qquad (2.5)$$

The Ekman layers which develop on the surfaces $z = 0$ and $z = 1$ "pump" and "suck" fluid from the interior of the fluid, thereby causing the

vertical velocities $w_1^{(1)}(x, y, 1)$ and $w_2^{(1)}(x, y, 0)$ to be non-zero. A relatively simple piece of analysis (see Appendix 1) shows that

$$w_1^{(1)}(x, y, 1) = -\frac{E^{\frac{1}{2}}}{2\varepsilon}\zeta_1^{(0)}(x, y, 1)$$

$$w_2^{(1)}(x, y, 0) = \frac{E^{\frac{1}{2}}}{2\varepsilon}\zeta_2^{(0)}(x, y, 0)$$

are reasonable representations of the Ekman pumping and suction effects, and since $\zeta_n^{(0)}$ are independent of z, these simplify to

$$\begin{aligned} w_1^{(1)}(x, y, 1) &= -\tfrac{1}{2}r\,\zeta_1^{(0)}(x, y) \\ w_2^{(1)}(x, y, 0) &= \tfrac{1}{2}r\,\zeta_2^{(0)}(x, y) \end{aligned} \qquad (2.6)$$

where $r = E^{\frac{1}{2}}/\varepsilon$.

A consideration of the dynamic boundary condition at the interface shows that the continuity of pressure p_n' across the interface demands that

$$h^{(0)} = \psi_2 - \psi_1 .$$

Using this along with (2.5) and (2.6) yields the equations of motion to first order in each layer, viz:

$$\left[\frac{\partial}{\partial t} + \frac{\partial\psi_1}{\partial x}\frac{\partial}{\partial y} - \frac{\partial\psi_1}{\partial y}\frac{\partial}{\partial x}\right]\left[\nabla^2\psi_1 + F(\psi_2 - \psi_1)\right] + \beta\frac{\partial\psi_1}{\partial x} = -r\nabla^2\psi_1$$

$$\left[\frac{\partial}{\partial t} + \frac{\partial\psi_2}{\partial x}\frac{\partial}{\partial y} - \frac{\partial\psi_2}{\partial y}\frac{\partial}{\partial x}\right]\left[\nabla^2\psi_2 - F(\psi_2 - \psi_1)\right] + \beta\frac{\partial\psi_2}{\partial x} = -r\nabla^2\psi_2$$

which we choose to write in the more convenient form

$$\frac{\partial q_p}{\partial t} + J(\psi_p, q_p) + \beta\frac{\partial\psi_p}{\partial x} = -r\nabla^2\psi_p \quad \text{for} \quad p = 1, 2 \qquad (2.7)$$

where $q_p = \nabla^2\psi_p \pm F(\psi_2 - \psi_1)$ with the upper sign for $p = 1$, and where $J(f, g) \equiv \frac{\partial f}{\partial x}\frac{\partial g}{\partial y} - \frac{\partial g}{\partial x}\frac{\partial f}{\partial y}$. These equations are known as the QUASI-GEOSTROPHIC POTENTIAL VORTICITY EQUATIONS.

2.2 Boundary conditions

To derive the boundary conditions for this system we require no normal flow at the boundaries $y = 0$ and $y = 1$, i.e. $v_p^{(0)} = 0$ at $y = 0, 1$. This condition requires, therefore, that

$$\frac{\partial \psi_p}{\partial x} = 0 \quad \text{on} \quad y = 0, 1 \quad \text{for} \quad p = 1, 2 . \tag{2.8}$$

In addition we require $v_p^{(1)} = 0$ on the same boundaries, and Phillips (1954) has shown that this introduces the condition that

$$\lim_{x\to\infty} \frac{1}{2x} \int_{-x}^{x} \frac{\partial^2 \psi_p}{\partial y \partial t}\, dx = 0 \quad \text{on} \quad y = 0, 1 \quad \text{for} \quad p = 1, 2 .$$

In particular, when the channel is assumed to have a periodicity of L_x, i.e. $\psi(x, y) = \psi(x + L_x, y)$, then this condition becomes

$$\frac{\partial}{\partial t} \int_{0}^{L_x} \frac{\partial \psi_p}{\partial y}\, dx = 0 \quad \text{on} \quad y = 0, 1 \quad \text{for} \quad p = 1, 2 \tag{2.9}$$

With these boundary conditions we may derive a consistency condition on the stream function for each layer; the derivation contained in Appendix 2 yields the condition

$$\iint_{\Omega} \zeta_p \, d\Omega = 0 \qquad \forall t \quad \text{and} \quad p = 1, 2$$

where $\Omega = \{(x, y) \in [0, L_x] \times [0, 1]\}$. Green's Theorem may be used to write this in the equivalent form

$$\left[\int_0^{L_x} \frac{\partial \psi_p}{\partial y} \, dx \right]_{y=0}^{1} = 0 \quad \forall t \quad \text{and} \quad p = 1, 2 \, .$$

It should also be pointed out that these boundary conditions are inviscid in the sense that they do not cause boundary layers on the sidewalls $y = 0, 1$ to form, as they would in the laboratory. Hart, in 1972, pointed out that these boundary layers are essentially passive, closing the circulation caused by the Ekman pumping and do not play a great role in the dynamics of the flow.

Equations (2.7) and the boundary conditions (2.8) and (2.9) constitute a well-posed initial value problem in the infinitely periodic channel, and can therefore be directly integrated using some suitable technique, the construction of which is carried out below.

2.3 The Construction of the Solution Procedure

Let us begin by rewriting the system in a semi-discrete form, treating time as the discrete variable: the two space dimensions, x and y, are for the present continuous. We may write the system, therefore, in the form

$$q^{n+1} = f(q_p^n, \psi_p^n)$$

$$q_p^n = \nabla^2 \psi_p^n \pm F(\psi_2^n - \psi_1^n) \qquad \text{for} \quad p = 1 \text{ and } 2$$

with the boundary conditions

$$\frac{\partial \psi_p^n}{\partial x} = 0$$

and

$$\int_0^{L_x} \frac{\partial \psi_p^n}{\partial y}\, dx = \text{constant} \quad \text{(specified by the initial conditions)}$$

on $y = 0$ and 1

with the periodicity condition $\psi_p(x, y) = \psi_p(x + L_x, y)$.

Hence, given initial stream functions, ψ_p^0 , we can use the prediction equation to derive values of q_p^1 everywhere in the region of Ω . This operation does not require the use of either boundary condition.

Then, having used the hyperbolic prediction equation, we use the elliptic equation to regain values of the stream function at the first time level. The inversion of the elliptic operator using both of the boundary conditions is well posed, and is carried out as follows: adding and subtracting the equations yields

$$\nabla^2(\psi_2 + \psi_1) = (q_2 + q_1) \quad .$$

$$\nabla^2(\psi_2 - \psi_1) - 2F(\psi_2 - \psi_1) = (q_2 - q_1)$$

with the boundary conditions

$$\frac{\partial}{\partial x}(\psi_2 \pm \psi_1) = 0 \quad \text{and} \quad \int_0^{L_x} \frac{\partial}{\partial y}(\psi_2 \pm \psi_1)dx = \text{const.} \quad \text{on} \quad y = 0 \text{ and } 1.$$

Take, for example, the second of these, the Helmholtz problem. We start by first solving the equation

$$(\nabla^2 - 2F)\hat{\psi}_D = q_D$$

with

$$\hat{\psi}_D = 0 \qquad \text{on} \quad y = 0, 1 \ ,$$

where the subscript D denotes the difference between the layer 2 and the layer 1 quantities.

Then for $\bar{\psi}_D = \psi_D - \hat{\psi}_D$ we have

$$(\nabla^2 - 2F)\bar{\psi}_D = 0$$

with

$$\bar{\psi}_D = \text{const.} \quad \text{(unknown)}$$

and

$$\int_0^{L_x} \frac{\partial \bar{\psi}_D}{\partial y}\, dx = \text{const.} \quad \text{(known)} \qquad \text{on} \quad y = 0,\ 1 \ .$$

It is clear that $\psi_D = \bar{\psi}_D(y)$ and that to find $\bar{\psi}_D$ we must solve the two-point boundary value problem

$$\frac{d^2\bar{\psi}_D}{dy^2} - 2F\bar{\psi}_D = 0$$

with $\dfrac{d\bar{\psi}_D}{dy}$ specified at $y = 0,\ 1$.

Hence we can derive values of ψ_D everywhere; a similar, but not identical procedure, exists for ψ_S (ψ_S being specified only as far as an arbitrary constant) and so in a semi-discrete sense we have a solution algorithm.

The fully discrete algorithm follows exactly the same principles: for the time discretisation leapfrog differencing is used, while central differences (see Fig. 7) are employed for the space derivatives on a regular rectangular mesh. The prediction equations (2.7), are therefore rewritten as: for $p = 1,\ 2$

$$D_{ot}\, Q_p^n = -\, J_h(\Psi_p^n,\, Q_p^n) - \beta D_{ox}\, \Psi_p^n - r[\nabla_h^2\, \Psi_p^n + \tfrac{1}{2}\theta\delta_t^2\, Q_p^n]$$

$$Q_p^n = \nabla_h^2\, \Psi_p^n \pm F(\Psi_2^n - \Psi_1^n) \qquad (2.10)$$

where

$$D_{ot}\, Q^n = \Delta_{ot}\, Q^n/\Delta t = \tfrac{1}{2}(Q^{n+1} - Q^{n-1})/\Delta t$$

$$\delta_t\, Q^n = Q^{n+\frac{1}{2}} - Q^{n-\frac{1}{2}}$$

$$\nabla_h^2\, \Psi^n = (\delta_x^2/\Delta x^2 + \delta_y^2/\Delta y^2)\Psi^n$$

and J_h is the approximation for the Jacobian term. The actual expression used for J_h was first derived by Arakawa in 1966, and is equivalent to using central differences to evaluate

$$\frac{1}{3}\left\{\left[\frac{\partial f}{\partial x}\frac{\partial g}{\partial y} - \frac{\partial f}{\partial y}\frac{\partial g}{\partial x}\right] + \left[\frac{\partial}{\partial x}\left(f\frac{\partial g}{\partial y}\right) - \frac{\partial}{\partial y}\left(f\frac{\partial g}{\partial x}\right)\right] - \left[\frac{\partial}{\partial x}\left(g\frac{\partial f}{\partial y}\right) - \frac{\partial}{\partial y}\left(g\frac{\partial f}{\partial x}\right)\right]\right\}.$$

This particular formulation of the Jacobian is energy and enstrophy conserving, and has been shown to reduce non-linear instabilities that occur in long time integrations of equations involving Jacobian terms.

It should also be noted that a "θ" term has been included to remove the growth of spurious solutions associated with the midpoint rule. Later we show that a necessary condition for stability is $\theta \geq 1$. With $\theta = 1$, this is a trapezium rule approximation for the dissipative term.

Given initial values of the stream function, values of vorticity, and hence Q_p can be calculated at all interior points, i.e. at all points in D_h (see Fig. 7). Actually on the boundary $y = 0$ or 1 we must devise some way of calculating the vorticity, $\zeta_p = \nabla^2\psi_p$. The simplest method,

which is, incidentally, consistent with the derivation of the Jacobian formulation being conservative of enstrophy as well as of energy, is to require $\zeta_p = 0$ on $y = 0, 1$. This condition in fact implies $\frac{\partial u_p}{\partial y} \simeq 0$ on $y = 0, 1$, and is equivalent to there being no boundary layers at the side wall.

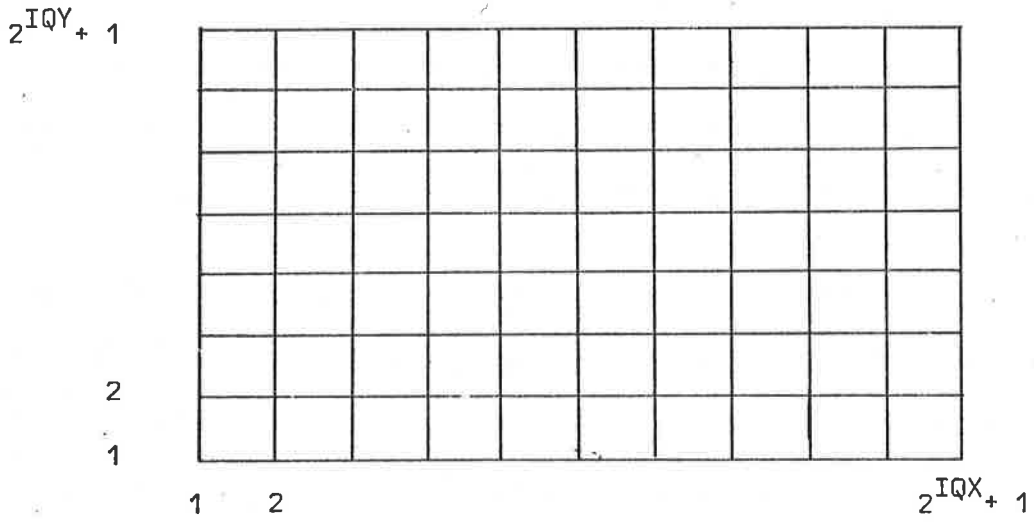

$$D_h = \{(i,j) : 1 \le i \le 2^{IQX}+1, 1 < j < 2^{IQY}+1\}$$

$$\Gamma_h = \{(i,j) : 1 \le i \le 2^{IQX}+1, j = 1 \text{ or } j = 2^{IQY}+1\}$$

Fig. 7 : The finite difference grid

An alternative boundary formulation would be to follow the method suggested by Roache (1972) : putting $\psi_{w+1} = \psi(x, \Delta y)$, the stream function evaluated one mesh point away from the wall, and $\psi_w = \psi(x, 0)$ then

$$\psi_{w+1} = \psi_w + \Delta y \left.\frac{\partial \psi}{\partial y}\right|_w + \frac{\Delta y^2}{2} \left.\frac{\partial^2 \psi}{\partial y^2}\right|_w + \frac{\Delta y^3}{6} \left.\frac{\partial^3 \psi}{\partial y^3}\right|_w$$

and

$$\psi_{w+2} = \psi_w + 2\Delta y \left.\frac{\partial \psi}{\partial y}\right|_w + 2\Delta y^2 \left.\frac{\partial^2 \psi}{\partial y^2}\right|_w + \frac{4}{3} \Delta y^3 \left.\frac{\partial^3 \psi}{\partial y^3}\right|_w .$$

Thus, taking a suitable linear combination of these we find that

$$\left.\frac{\partial^2\psi}{\partial y^2}\right|_w = \delta y^2(\psi_{w+1})/\Delta y^2 + O(\Delta y) .$$

Hence since $\left.\frac{\partial\psi}{\partial x}\right|_w = 0$,

$$\zeta_w = \delta y^2(\psi_{w+1})/\Delta y^2$$

is a first order approximation to ζ at the boundary. Obviously, by using more mesh points higher order approximations may be derived. Unfortunately this formulation has been found to be unstable.

At this stage we apply the prediction equation (2.10) to obtain values of Q_p^n at all points of D_h . The time discretisation being a two step method required some starting procedure for the first step. This is, typically, an Euler predictor with a Crank-Nicolson or fully implicit corrector applied five or more times to obtain good starting values. This is then sufficient to allow us to solve for Ψ_p^n at every point in $D_h \cup \Gamma_h$ in the way described above; the integral constraint is evaluated using some quadrature rule such as Simpson's rule with a third order approximation to $\left.\frac{\partial\psi}{\partial y}\right|_w$. The inversion of $(\nabla^2 - 2F)\Psi = Q$ uses Fast Fourier Transforms, which have been kindly provided by Professor Hockney in his program POT 1 (1970). An outline of this procedure is given in Appendix 3. Some form of diagnostic information can now be extracted before the next time step is performed.

3. LINEAR THEORY OF THE DIFFERENTIAL EQUATION

It is important to understand how the differential equation behaves when the wave amplitude is very small. To analyse the behaviour of such small perturbations we proceed as follows:

Into the differential equation (2.7) substitute $\psi_p = \mp U_y + \phi_p$ $(p = 1, 2)$, where $\mp U_y$ is an exact solution of the system and represents the basic, unperturbed state and where $|\phi_p| << U$. Thus ignoring terms involving products of the ϕ_p and their derivatives, we derive a system of linearised equations, namely

$$\left[\frac{\partial}{\partial t} \pm U \frac{\partial}{\partial x}\right]\left[\nabla^2\phi_p \pm F(\phi_2 - \phi_1)\right] + \frac{\partial \phi_p}{\partial x}(\beta \pm 2FU) = -r\nabla^2\phi_p$$

for $p = 1$ and 2. (3.1)

We examine these using a Fourier mode of the form

$$\gamma\phi_1 = \phi_2 = A\gamma e^{ik_x(x-it)} \sin k_y y , \qquad (A, \gamma, c \in \mathbb{C})$$

where $k_x = 2\pi\ell/L_x$, $k_y = m\pi$ and ℓ and m are positive integers; substituting this into (3.1) gives

$$ik_x\{(-c \pm U)(-k^2\phi_p \pm F(\phi_2 - \phi_1)) + (\beta \pm 2FU)\phi_p\} - rk^2\phi_p = 0 , \quad (p = 1, 2)$$

that is

$$\begin{bmatrix} [(k^2 + F)(c - U) + (\beta + 2FU)]ik_x - rk^2 & -F(c - U)ik_x \\ -F(c + U)ik_x & [(k^2 + F)(c + U) + (\beta - 2FU)]ik_x - rk^2 \end{bmatrix} \underline{\phi} = \underline{0} \quad (3.2)$$

where $\underline{\phi} = \begin{bmatrix} \phi_1 \\ \phi_2 \end{bmatrix}$.

The first of these equations can be used to give an expression for γ, the quantity which represents the phase shift and/or amplification between wave modes in each layer, namely

$$\gamma = \frac{[k^2(c - U) + F(c + U) + \beta] + i[rk^2/k_x]}{F(c - U)} \qquad (3.3)$$

Setting the determinant in (3.2) equal to zero yields a quadratic equation for c, namely

$$c^2[k^2(k^2 + 2F)] + 2c[(k^2 + F)\beta + irk^2(k^2 + F)/k_x]$$

$$+ [(\beta + irk^2/k_x)^2 - k^2U^2(k^2 - 2F)] = 0 \qquad (3.4)$$

$$\text{i.e.} \quad c = -\left(\frac{k^2 + F}{k^2 + 2F}\right)\left(\frac{\beta}{k^2} + \frac{ir}{k_x}\right) \pm \frac{(k^4U^2(k^4 - 4F^2) + F^2(\beta + irk^2/k_x)^2)^{\frac{1}{2}}}{k^2(k^2 + 2F)} \qquad (3.5)$$

We now need to derive expressions for growth rate, positions of marginal curves between regions of linearly stable and linearly unstable modes and expressions for γ : the general case for the difference scheme being somewhat intractable, we consider each of the cases

(A) $r = 0$; $\beta = 0$

(B) $r = 0$; $\beta \neq 0$

(C) $r \neq 0$; $\beta = 0$

in preparation for comparison with the theory of the difference scheme. The growth rate of the Fourier mode is just $k_x c_I$, where $c_I = \text{Im } c$, and so regions of growth are characterised by $c_I > 0$ if we always suppose $k_x > 0$.

(A) $r = 0$; $\beta = 0$

Equation (3.4) becomes

$$c^2 = U^2 \frac{(k^2 - 2F)}{(k^2 + 2F)} \quad ; \qquad (3.A.1)$$

so the growing modes are those of lowest wave number $k^2 < 2F$, and it is this that defines the curve of marginal stability. (3.A.2)

For growing modes

$$c_I = U\left\{\frac{2F - k^2}{2F + k^2}\right\}^{\frac{1}{2}} \qquad (3.A.3)$$

and $$\gamma \equiv \phi_2/\phi_1 = \frac{k^2 + F}{F} + \frac{2U}{(c - U)} \qquad (3.A.4)$$

$$= \frac{c + U}{c - U} + \frac{k^2}{F} \quad .$$

Note that $\gamma = e^{i\pi/2}$ for $k^2 = 0$ and $\gamma = 1$ for $k^2 = 2F$.

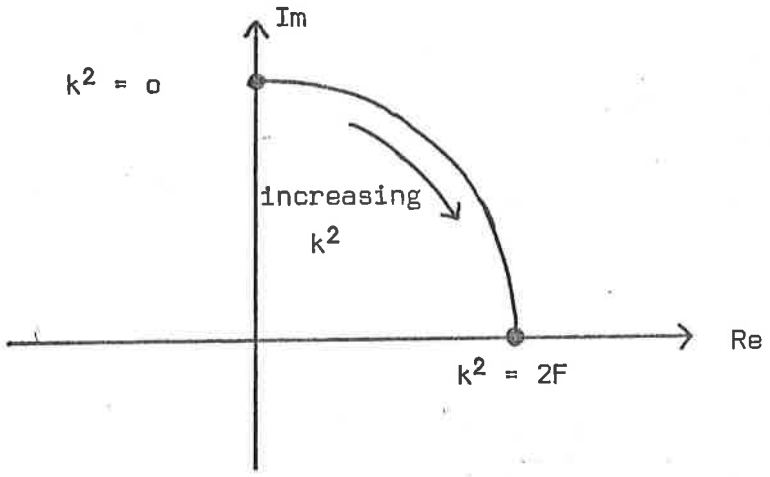

Sketch of path of γ for increasing k^2

(B) $r = 0 \; ; \; \beta \neq 0$

For $r = 0$, equation (3.4) becomes

$$c^2[k^2(k^2 + 2F)] + 2c\beta k^2 + (\beta^2 - k^2U^2(k^2 - 2F)) = 0 \qquad (3.B.1)$$

so that $$c = -\left(\frac{k^2 + F}{k^2 + 2F}\right)\frac{\beta}{k^2} \pm \frac{[k^4U^2(k^4 - 4F^2) + F^2\beta^2]^{\frac{1}{2}}}{k^2(k^2 + 2F)} \; .$$

Thus the growing modes are given by

$$k^4(4F^2 - k^4) > \frac{F^2\beta^2}{U^2} \; . \qquad (3.B.2)$$

Note that for there to exist any growing modes it is necessary that

$4F^4 > F^2\beta^2/U^2$

i.e. $U > U_c = \beta/_{2F}$.

The value of c_I for a growing mode is

$$c_I = \frac{(k^4U^2(4F^2 - k^4) - F^2\beta^2)^{\frac{1}{2}}}{k^2(k^2 + 2F)} \qquad (3.B.3)$$

and

$$\gamma = \frac{k^2(c - U) + \beta + F(c + U)}{F(c - U)} \qquad (3.B.4)$$

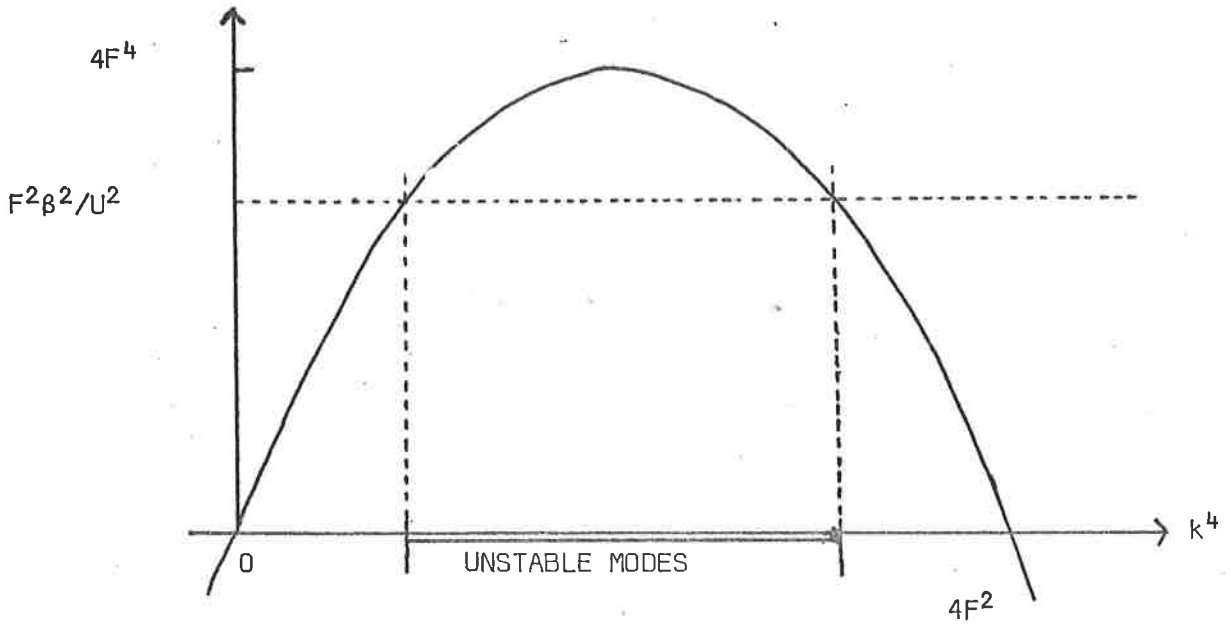

Sketch indicating unstable modes for $r = 0$, $\beta \neq 0$.

(C) $r = O(1)$; $\beta = 0$

For $r = O(1)$ equation (3.4) reduces to

$$c^2[k^2(k^2 + 2F)] + 2c[irk^2(k^2 + F)/k_x] + [- k^2U^2(k^2 - 2F) - r^2k^4/k_x^2] = 0 \qquad (3.C.1)$$

so that

$$C = - \left(\frac{k^2 + F}{k^2 + 2F}\right) \frac{ir}{k_x} + \frac{[U^2(k^4 - 2F^2) - F^2r^2/k_x^2]^{\frac{1}{2}}}{(k^2 + 2F)} .$$

For growing modes we need

$$U^2(4F^2 - k^4) + F^2r^2/k_x^2 > (k^2 + F)^2r^2/k_x^2$$

i.e. $$U^2(2F - k^2) > k^2r^2/k_x^2$$

i.e. $$\frac{k_x^2}{k^2}(2F - k^2) > \frac{r^2}{U^2} . \qquad (3.C.2)$$

Note that for any modes to grow we need $U > U_c = r/\sqrt{2F}$: for such modes

$$c_I = - \frac{r}{k} \left(\frac{k^2 + F}{k^2 + 2F}\right) + \frac{(U^2(4F^2 - k^4) + F^2r^2/k_x^2)^{\frac{1}{2}}}{(k^2 + 2F)} \qquad (3.C.3)$$

and $$\gamma = \frac{[k^2(c - U) + F(c + U)] + i[rk^2/k_x]}{F(c - U)} \qquad (3.C.4)$$

Note that the curve of marginal stability is defined by

$U^2 = r^2k^2/[k_x^2(2F - k^2)]$, and hence on this curve

$$\gamma = \frac{k^2 - F}{F} - ik \frac{\sqrt{2F - k^2}}{F}$$

$$\Rightarrow |\gamma|^2 = \frac{(k^2 - F)^2}{F^2} + k^2 \frac{(2F - k^2)}{F^2} = 1 .$$

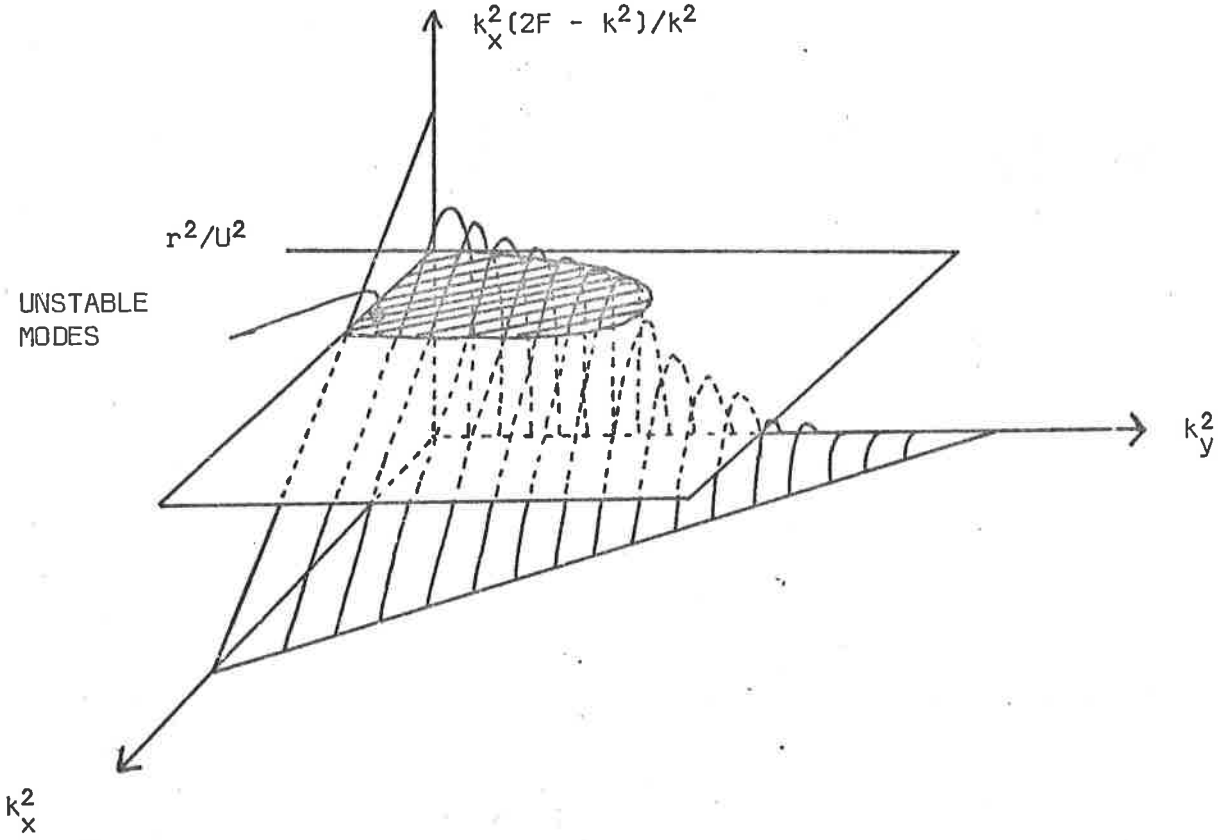

Sketch indicating unstable modes
for $r \neq 0$, $\beta = 0$

4. LINEAR THEORY OF THE DIFFERENCE SCHEME

We linearise the difference scheme in a way exactly analogous to that for the differential equations; i.e. we substitute $\Psi_p = \mp U_y + \Phi_p$ into the difference scheme and ignore all terms involving products of Φ_p and their derivatives. The linearised difference scheme is, therefore

$$(D_{ot} \pm UD_{ox})\overline{Q}_p^n + D_{ox}\Phi_p^n(\beta \pm 2FU) = -r(\nabla_h^2\Phi_p^n + \tfrac{1}{2}\theta\,\delta_t^2 Q_p^n) \quad (p = 1, 2) \quad (4.1)$$

where $\overline{Q}_p^n = \nabla_h^2\Phi_p^n \pm F(\Phi_2^n - \Phi_1^n)$.

As with the differential equation, we can now examine the linear characteristics of the difference scheme using a Fourier Mode, except that now we use the discrete mode given by

$$\gamma^h\Phi_1^n = \Phi_2^n = A^h\gamma^h e^{ik_x(\ell\Delta x - Cn\Delta t)} \sin k_y m\Delta y \qquad (4.2)$$

where the triple $(\ell\Delta x, m\Delta y, n\Delta t)$ defines a discrete point corresponding to (x, y, t) . Here A^h and γ^h represent the finite difference equivalents to A and γ in the differential equation; C is the phase speed corresponding to c .

Substituting the discrete Fourier mode into the four difference operators which appear in equation (4.1) we can define K^2, K_x, C_λ and ε as follows:

$$\nabla_h^2\Phi_p^n = -\left\{\left(\frac{\sin \tfrac{1}{2}k_x\Delta x}{\tfrac{1}{2}\Delta x}\right)^2 + \left(\frac{\sin \tfrac{1}{2}k_y\Delta y}{\tfrac{1}{2}\Delta y}\right)^2\right\}\Phi_p^n \equiv -K^2\Phi_p^n$$

$$D_{ox}\Phi_p^n = i\left(\frac{\sin k_x\Delta x}{\Delta x}\right) \equiv iK_x\Phi_p^n \qquad (4.3)$$

$$D_{ot}\Phi_p^n = \tfrac{1}{2}(\lambda - \lambda^{-1})\,\Phi_p^n/\Delta t \equiv -iK_xC_\lambda\Phi_p^n$$

$$\tfrac{1}{2}\,\delta_t^2\Phi_p^n = \tfrac{1}{2}(\lambda - 2 + \lambda^{-1})\,\Phi_p^n \equiv \varepsilon\Phi_p^n$$

where

$$\lambda = \exp(-ik_x C\Delta t) .$$

We can observe that as $\Delta t \to 0$ (k_x fixed), then

$$K^2 \to k^2$$

$$K_x \to k_x$$

$$C_\lambda \to C \to c$$

$$\varepsilon \to 0 ,$$

where ε is a function of λ and hence is dependent upon C, and that we can resolve all modes such that

$$-\pi \leq k_x \Delta x \leq \pi$$

$$-\tfrac{1}{2}\pi \leq k_y \Delta y \leq \tfrac{1}{2}\pi .$$

In the analysis which follows we shall assume that k_x and k_y are positive; we shall also solve for C_λ and then obtain λ from

$$\lambda + 2iK_x C_\lambda \Delta t\lambda - 1 = 0 \qquad (4.4)$$

Substituting (4.3) into the linearised difference scheme (4.1) the following pair of equations is derived:

$$\{-iK_x C_\lambda \pm iK_x U\}\{-K^2\Phi_p^n \pm F(\Phi_2^n - \Phi_1^n)\} + iK_x(\beta \pm 2FU)\Phi_p^n$$

$$+ r[-K^2\Phi_p^n + \varepsilon\theta(-K^2\Phi_p^n \pm F(\Phi_2^n - \Phi_1^n))] = 0 \qquad (p = 1, 2)$$

and denoting $[\Phi_1^n, \Phi_2^n]^T$ by $\underline{\Phi}^n$, this can be rewritten in the form:

$$\begin{bmatrix} iK_x(\beta + 2FU) + i(K_xC_\lambda - K_xU)(K^2 + F) & -i(K_xC_\lambda - K_xU)F \\ - rK^2 - r\theta\varepsilon(K^2 + F) & + r\theta\varepsilon F \\ \\ - i(K_xC_\lambda + K_xU)F & iK_x(\beta - 2FU) + i(K_xC_\lambda + K_xU)(K^2 + F) \\ + r\theta\varepsilon F & - rK^2 - r\theta\varepsilon(K^2 + F) \end{bmatrix} \underline{\Phi}^n = \underline{0}$$

The first of these equations can be used to give the value of γ^h, namely

$$\gamma^h = \frac{iK_x(\beta + 2FU) + i(K_xC_\lambda - K_xU)(K^2 + F) - rK^2 - r\theta\varepsilon(K^2 + F)}{i(K_xC_\lambda - K_xU)F - r\theta\varepsilon F}$$

$$= \frac{[K^2(C_\lambda - U) + F(C_\lambda + U) + \beta] + i[rK^2/K_x + r\theta\varepsilon(K^2 + F)/K_x]}{F(C_\lambda - U + ir\theta\varepsilon/K_x)} \quad (4.5)$$

Requiring a non-trivial solution for $\underline{\Phi}^n$ yields an equation for C_λ, namely

$$C_\lambda^2[K^2(K^2 + 2F)] + 2C_\lambda[\beta(K^2 + F) + irK^2(K^2 + F + \varepsilon\theta(K^2 - 2F))/K_x]$$

$$+ [(\beta + \frac{irK^2}{K_x})^2 - U^2K^2(K^2 - 2F) + \frac{r\theta\varepsilon}{K_x^2}(2(\beta iK_x - rK^2)(K^2 + F) - r\theta\varepsilon K^2(K^2 + 2F))] = 0 \quad (4.6)$$

and it is important to note that this is an equation for C_λ and not C. Furthermore, as noted above, ε depends on λ (or C) and so when $r \neq 0$ we must look at the quartic for λ directly without first obtaining an expression for C_λ.

We now want to demonstrate L-R stability for the difference scheme, and derive results for growth rate and stability boundaries for comparison with the results for the differential equation; again, it is most convenient to consider the cases

(A) $r = 0$; $\beta = 0$

(B) $r = 0$; $\beta \neq 0$

(C) $r \neq 0$; $\beta = 0$

Before we do this, however, we give conditions for the roots of

$$\lambda^2 + 2b\lambda - 1 = 0 \qquad (b \in \mathbb{C})$$

to be contained within the circle of radius $1 + K\Delta t$, i.e. $|\lambda| \leq 1 + K\Delta t$. This will greatly help the analysis of equation (4.4).

(i) $b = b_R$: $|b_R| \leq 0(\Delta t)$

(ii) $b = ib_I$: $|b_I| \leq 1 + 0(\Delta t^2)$

(iii) $b = b_R + ib_I$: $|\lambda| \leq 1 + K\Delta t$ iff $(1 + K\Delta t)^2\mu^2 + 2b(1 + K\Delta t)\mu - 1 = 0$ has all its roots in the unit circle. Miller's criterion gives

(a) when $K = 0$, $b_R = 0$ and $|b_I| \leq 1$

(b) when $K > 0$, $\left|b_R(1 + 2K\Delta t) - 2ib_IK\Delta t(1 - \frac{3}{2} K\Delta t)\right| \leq$

$$K\Delta t(1 + \tfrac{3}{2} K\Delta t) + 0(\Delta t^3)$$

i.e. $|b_R - 2ib_IK\Delta t| \leq 0(\Delta t)$.

(A) $r = 0$; $\beta = 0$

For flow with these parameters equation (4.6) reduces to

$$C_\lambda^2K^2(K^2 + 2F) - U^2K^2(K^2 - 2F) = 0$$

giving

$$C_\lambda = \pm \left(\frac{K^2 - 2F}{K2 + 2F}\right)^{\frac{1}{2}} \qquad (4.A.1)$$

(i) L-R Stability

For Lax-Richtmeyer stability we require $|\lambda| = 1 + O(\Delta t)$. Using the conditions we derived for the zeros of $\lambda^2 + 2\lambda b - 1$ we can say the following:

(a) Whenever $K^2 > 2F$, C_λ is real from (4.A.1) and λ in (4.4) is $1 + O(\Delta t)$ only if

$$|K_x C_\lambda \Delta t| \leq 1 + O(\Delta t^2) .$$

Substituting in here for C_λ we require

$$0 \leq \sin^2(k_x \Delta x) \left[U \frac{\Delta t}{\Delta x}\right]^2 \left(\frac{K^2 - 2F}{K^2 + 2F}\right) \leq 1 + O(\Delta t^2)$$

and when $k_x \Delta x = \frac{\pi}{2}$ as $\Delta x \to 0$, this condition yields the familiar CFL criterion

$$U \frac{\Delta t}{\Delta x} \leq 1 ,$$

and the time step is bounded by $\Delta x/U$.

(b) Whenever $K^2 < 2F$, C_λ is purely imaginary and we can conclude from (4.A.1) that $|\lambda| = 1 + O(\Delta t)$ because

$$|K_x C_\lambda \Delta t| = K_x U \Delta t \left(\frac{2F - K^2}{2F + K^2}\right)^{\frac{1}{2}} \leq (2F)^{\frac{1}{2}} U \Delta t = O(\Delta t) .$$

(ii) growth rates and position of neutral curve

We now wish to find the region in which there is no growth, i.e. regions in which $|\lambda| \leq 1$. This occurs, from the analysis of (4.4). only when $C_\lambda \in \mathbb{R}$, i.e. when $K^2 > 2F$. There is growth for the lowest wave modes given by

$$K^2 < K_c^2 = 2F \ . \qquad (4.A.2)$$

Then C_λ is entirely imaginary, and so λ is entirely real and (4.A.1), (4.3) imply

$$e^{k_x C_I \Delta t} - e^{-k_x C_I \Delta t} = -2iK_x C_\lambda \Delta t = 2UK_x \Delta t \left(\frac{2F - K^2}{2F + K^2}\right)^{\frac{1}{2}}$$

$$\Rightarrow k_x C_I = K_x U \left(\frac{2F - K^2}{2F + K^2}\right)^{\frac{1}{2}} + O(\Delta t^2) \qquad (4.A.3)$$

We can also note that (4.5) implies that γ^h, the phase shift between the two layers, is given by

$$\gamma^h \equiv \Phi_2/\Phi_1 = \frac{K^2(C_\lambda - U) + F(C_\lambda + U)}{F(C_\lambda - U)} \qquad (4.A.4)$$

(iii) positioning of spurious modes

For each value of C_λ we have derived there are two values of λ and hence, since there are two values of C_λ there are two spurious modes. Can we be sure that we will not be troubled by these spurious modes growing faster than the physical modes (i.e. relative instability)? We show that we can.

When there are growing modes, a little algebra gives the four values of λ to be

$$\lambda_1 \sim 1 + k_x|C_\lambda|\Delta t \qquad \text{as} \quad \Delta t \to 0$$

$$\lambda_2 = \frac{-1}{\lambda_1} \sim -1 + k_x|C_\lambda|\Delta t \qquad \text{as} \quad \Delta t \to 0$$

$$\lambda_3 = 1 - k_x|C_\lambda|\Delta t \qquad \text{as} \quad \Delta t \to 0$$

$$\lambda_4 = \frac{-1}{\lambda_3} \sim -1 - k_x|C_\lambda|\Delta t \qquad \text{as} \quad \Delta t \to 0$$

Here λ_1 and λ_3 represent the true modes while λ_2 and λ_4 represent the computational modes. In fact $\lambda_1 = -\lambda_4$ and $\lambda_2 = -\lambda_3$. Hence the true part of the growing mode and the spurious part of the decaying mode grow at the same rate: similarly the true part of the decaying mode and the spurious part of the growing mode decay at the same rate.

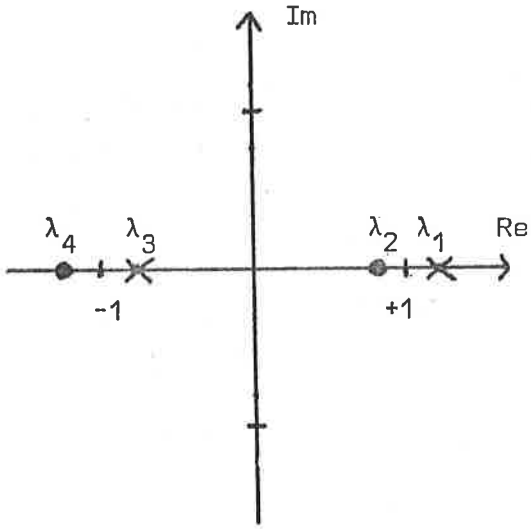

The conclusion is that neither spurious mode upsets the computation.

(B) $r = 0$; $\beta \neq 0$

For flow with these parameters the equation for C_λ, (4.6), reduces to

$$C_\lambda^2 K^2(K^2 + 2F) + 2C_\lambda(K^2 + F) + (\beta^2 - U^2K^2(K^2 - 2F)) = 0$$

$$\Rightarrow \quad C_\lambda = -\left\{\left(\frac{K^2 + F}{K^2 + 2F}\right)\frac{\beta}{K^2} \pm \frac{[U^2K^4(K^4 - 4F^2) + F^2\beta^2]^{\frac{1}{2}}}{K^2(K^2 + 2F)}\right\} \qquad (4.B.1)$$

(i) L-R Stability

Following the same procedure as in Section (A) we look at the following two cases:

(a) C_λ is real if $K^4(4F^2 - K^4) \leq F^2\beta^2/U^2$ in which case stability requires $|K_x C_\lambda \Delta t| \leq 1 + O(\Delta t^2)$. Now

$$|K_x C_\lambda \Delta t| \leq K_x \Delta t \left[\frac{(K^2 + F)\beta + UK^2|K^4 - 4F^2|^{\frac{1}{2}} + F\beta}{(K^2 + 2F)K^2}\right]$$

$$\leq K_x \Delta t \left[\frac{\beta}{K^2} + U\right]$$

$$\leq \Delta t\,[UK_x + \beta/K_x] \ .$$

Clearly $\Delta t[UK_x + \beta/K_x] \le 1 + O(\Delta t^2)$ as $\Delta t \to 0$ unless $K_x \to 0$ or $K_x \to \infty$: however we have

$$K_x = \frac{\sin k_x \Delta x}{\Delta x} \ge \frac{2}{\pi} k_x .$$

and k_x is bounded below by $\frac{2\pi}{L_x}$ where L_x is the length of the channel; so we can assume that $K_x^{-1} = O(\Delta t)$ and since $K_x \le (\Delta x)^{-1}$ we have

$$\Delta t[UK_x + \beta/K_x] \le 1 + O(\Delta t^2) \quad \text{if} \quad U\frac{\Delta t}{\Delta x} \le 1 .$$

(b) C_λ is complex in the small range of K values given by

$$K^4(4F^2 - K^4) \ge F^2\beta^2/U^2 .$$

Thus for all Δx K is uniformly bounded both above and below and it is easy to show that

$$Re(K_x C_\lambda \Delta t) = 1 + O(\Delta t^2) , \quad Im(K_x C_\lambda \Delta t) \le O(\Delta t) \quad \text{as} \quad \Delta t \to 0 .$$

(ii) growth rates and position of neutral curve

As in Case (A) we now wish to determine the region in which there are no growing modes. The criterion is again $C_\lambda \in \mathbb{R}$ for $|\lambda| \le 1$; i.e. there is growth for the lowest wave number modes given by

$$K^4(4F^2 - K^4) > F^2\beta^2/U^2 \qquad (4.B.2)$$

Now, however, C_λ has both a real and an imaginary part and (4.B.1) and (4.3) imply

$$e^{-ik_x C\Delta t} - e^{+ik_x C\Delta t} = -2iK_x C_\lambda \Delta t$$

$$= 2iK_x \Delta t\left\{\left(\frac{K^2 + F}{K^2 + 2F}\right)\frac{\beta}{K^2} - i\,\frac{[U^2K^4(4F^2 - K^4) - \beta^2F^2]^{\frac{1}{2}}}{K^2(K^2 + 2F)}\right\} .$$

Comparing real and imaginary parts implies:

$$\cos(k_x C_R \Delta t)[e^{k_x C_I \Delta t} - e^{-k_x C_I \Delta t}] = 2K_x \Delta t [U^2K^4(4F^2 - K^4) - \beta^2F^2]^{\frac{1}{2}}/(K^2(K^2 + 2F))$$

$$= 2K_x \Delta t \, Re(C_\lambda)$$

and $$\sin(k_x C_R \Delta t)[e^{k_x C_I \Delta t} + e^{-k_x C_I \Delta t}] = - 2K_x \Delta t \left(\frac{K^2 + F}{K^2 + 2F}\right) \frac{\beta}{K^2}$$

$$= - 2K_x \Delta t \, Im(C_\lambda) \, .$$

These give

$$C_I = \Gamma \, . \, [U^2K^2(4F^2 - K^4) - F^2\beta^2]^{\frac{1}{2}}/(K^2(K^2 + 2F)) \qquad (4.B.3)$$

where $\Gamma = \sec\{\sin^{-1}(K_x \Delta t \, Re(C_\lambda))\} + O(\Delta t^2)$.

Here $\Gamma = 1 + O(\Delta t)$, and in practice $|1 - \Gamma| \leq 10^{-2}$.

Finally we may observe that (4.5) implies that the phase multiplier γ^h is given by

$$\gamma^h = \frac{K^2(C_\lambda - U) + F(C_\lambda + U) + \beta}{F(C_\lambda - U)} \qquad (4.B.4)$$

(iii) positioning of spurious modes

Again there are only 2 true modes and there are 2 spurious modes. Proceeding in exactly the same way as before we can conclude that the four values for λ are :

$$\begin{cases} \lambda_1 \sim 1 + |K_x C_{\lambda I}|\Delta t + i|K_x C_{\lambda R}|\Delta t & \text{as } \Delta t \to 0 \\ \lambda_2 = \dfrac{1}{\lambda_1} \sim - 1 + |K_x C_{\lambda I}|\Delta t + i|K_x C_{\lambda R}|\Delta t & \text{as } \Delta t \to 0 \end{cases}$$

$$\begin{cases} \lambda_3 \sim 1 - |K_x C_{\lambda I}|\Delta t + i|K_x C_{\lambda R}|\Delta t & \text{as } \Delta t \to 0 \\ \lambda_4 = \dfrac{1}{\lambda_3} \sim -1 - |K_x C_{\lambda I}|\Delta t + i|K_x C_{\lambda R}|\Delta t & \text{as } \Delta t \to 0 \end{cases}$$

where $C_\lambda = C_{\lambda R} \pm iC_{\lambda I}$.

A brief reference to the sketch of the positions of λ_1, λ_2, λ_3, λ_4 will enable us to draw the same conclusions as were made before in Case (A), although now the phase speed along the channel will (to $O(\Delta t)$) be the same for all waves.

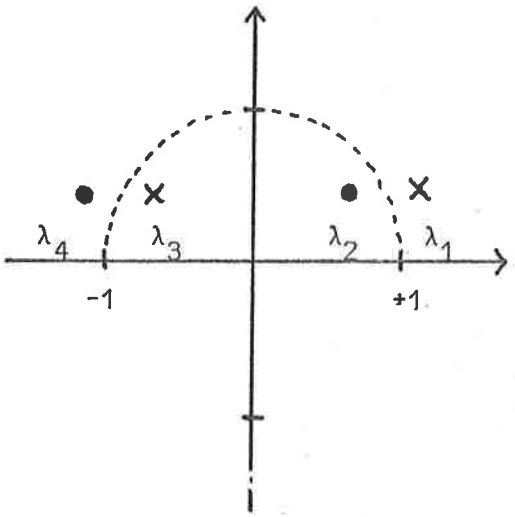

(C) $r \neq 0$; $\beta = 0$

This is the hardest of the three cases we wish to study, the difficulty largely arising out of the "θ" term used in the stability of the dissipative term. Equation (4.6) gives the following relationship for C_λ and ε .

$$C_\lambda^2(K^2 + 2F) + 2C_\lambda\left[\frac{ir}{K_x}(K^2 + F) + \frac{ir\theta}{K_x}\varepsilon(K^2 + 2F)\right]$$

$$+ \left[-\frac{r^2K^2}{K_x^2} - U^2(K^2 - 2F) - \frac{r\theta\varepsilon}{K_x^2}(2r(K^2 + F) + r\varepsilon\theta(K^2 + 2F))\right] = 0 .$$

As previously noted both C_λ and ε depend on λ and hence on C , although $\varepsilon << 1$ and tends to zero as Δt becomes small. It is therefore

best to use the definitions of C_λ and ε in (4.3) to rewrite this as a quartic in λ, viz:

$$\lambda^4(1 + r\theta\Delta t)^2 + 4\lambda^3(1 + r\theta\Delta t)r\Delta t \left[\left(\frac{K^2 + F}{K^2 + 2F}\right) - \theta\right]$$
$$+ (1 - r\theta\Delta t)^2 - 4\lambda(1 - r\theta\Delta t)r\Delta t \left[\left(\frac{K^2 + F}{K^2 + 2F}\right) - \theta\right]$$
$$+ \lambda^2\{-2(1 - r^2\theta^2\Delta t^2) + 4K_x^2U^2 \left(\frac{K^2 - 2F}{K^2 + 2F}\right)\Delta t^2$$
$$+ 4\frac{(1 - \theta)r^2}{K^2 + 2F}\Delta t^2 \{K^2(1 - \theta) - 2F\theta\}\} = 0$$

which factorises to

$$\{\lambda^2(1 + r\theta\Delta t) - (1 - r\theta\Delta t)\}\{\lambda^2(1 + r\theta\Delta t) + 4r\Delta t\lambda \left[\left(\frac{K + F}{K + 2F}\right) - \theta\right]$$
$$- (1 - r\theta\Delta t)\} + 4\Delta t^2\lambda^2 \{K_x^2U^2 \left(\frac{K^2 - 2F}{K^2 + 2F}\right)$$
$$+ \frac{(1 - \theta)r^2}{K^2 + 2F}\{K^2(1 - \theta) - 2F\theta\}\} = 0. \qquad (4.C.1)$$

We write this as

$$p_2(\lambda)\, q_2(\lambda) + A\lambda^2 = 0$$

where A depends on U, Δt, k_x, Δx, Δy, k_y, F, r, θ. To show L-R stability we must show that the roots of this equation can be bounded by $1 + M\Delta t$ uniformly as $\Delta t \to 0$ with $\frac{\Delta x}{\Delta t}$ in some refinement set.

Clearly, the zeros of $p_2(\lambda)\, q_2(\lambda)$ must be situated somewhere near the zeros of $p_2(\lambda)\, q_2(\lambda) + A\lambda^2$ for the sums and products of the roots for the two functions are the same. It is therefore prudent to examine $p_2(\lambda)\, q_2(\lambda)$ first before the $A\lambda^2$ term is added.

The zeros of $p_2(\lambda)\, q_2(\lambda)$ are found easily: those of $p_2(\lambda)$ are situated at

$$\lambda = \pm \left\{\frac{1 - r\,\Delta t}{1 + r\,\Delta t}\right\}^{\frac{1}{2}}$$

and are therefore real and situated within the unit disc; but those of $q_2(\lambda)$ are more complicated, namely

$$\lambda_{\pm} = [-2r\Delta t\left(\frac{K^2 + F}{K2 + 2F} - \theta\right) \pm (1 + r^2\Delta t^2(4\left(\frac{K^2 + F}{K2 + 2F} - \theta\right)^2 - \theta^2))^{\frac{1}{2}}]/(1 + r\theta\Delta t).$$

We can deduce that because $\frac{K^2 + F}{K^2 + 2F} \leq 1 \quad \forall\ k_x, k_y, \Delta x, \Delta y,$

$$|\lambda_{\pm}| < 1 + M_{\pm}(r, F, \theta)\Delta t, \quad \text{where } M_{\pm} \text{ are independent of } \Delta x, \Delta y, k_x, k_y.$$

When $\theta \geq 1$, we can go further and say that

$$\lambda_+ = 1 + \frac{2r\Delta t}{K^2 + 2F}(K^2(\theta - 1) + F\theta) + O(\Delta t^2) > 1$$

and $$\lambda_- = -1 + \frac{2r\Delta t}{K^2 + 2F}(K^2(\theta - 1) + F\theta) + O(\Delta t^2) > -1 .$$

The effect of adding $A\lambda^2$ to $p_2(\lambda)\, q_2(\lambda)$ to get $p_2(\lambda)\, q_2(\lambda) + A\lambda^2 = 0$ is now clear (see Fig. 8): the roots r_1 and r_2 move closer together when $A > 0$ as do r_3 and r_4 : the converse is true when $A < 0$. There is also some critical value of A, A_0 say, $(A_0 > 0)$ above which the zeros of $p_2(\lambda)\, q_2(\lambda) + A\lambda^2$ all lie or within the unit disc. If $A < A_0$, the root at r_1 (and possibly r_4) will be outside the unit circle, and to show L-R stability we must show that $r_1 < 1 + M\Delta t$ uniformly. We need not consider r_4 since $|r_1| > |r_4|$.

Referring to the enlargement of $p_2q_2 + A\lambda^2$ near $\lambda = +1$ (Fig. 9), we can say that

$$\xi \leq \eta/f'(1)$$

where

$$f(\lambda) = p_2(\lambda)\, q_2(\lambda) + A\lambda^2.$$

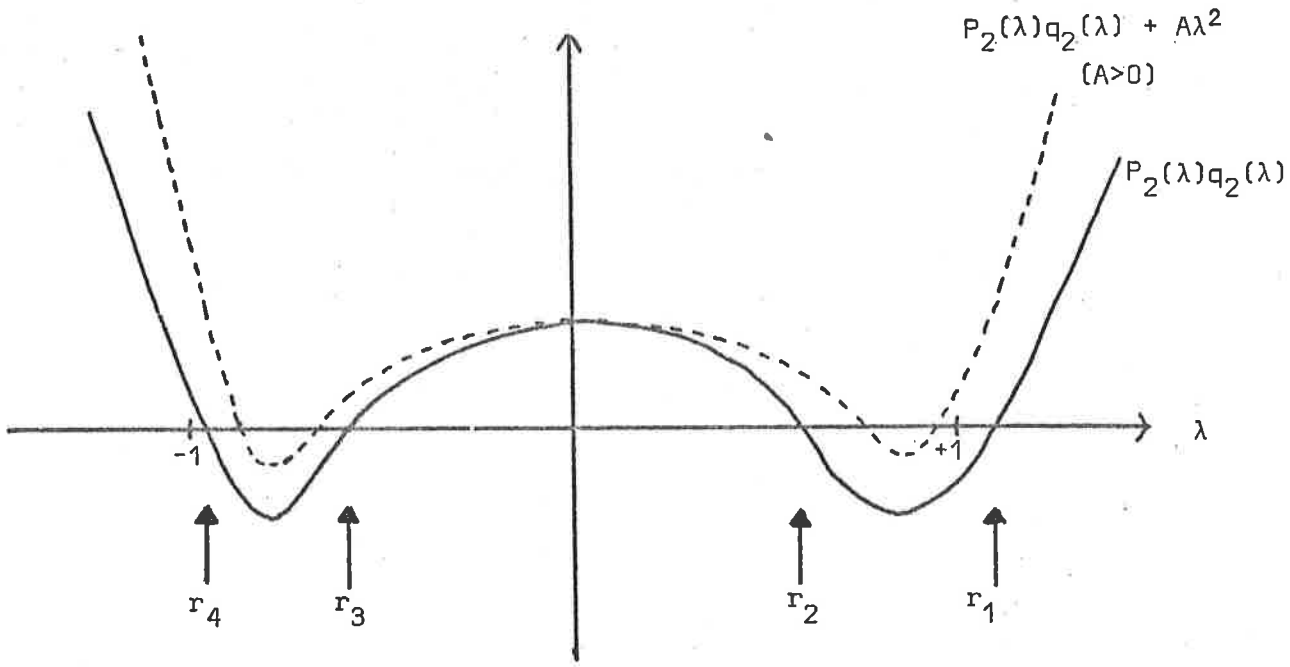

Fig. 8 : Sketch of $P_2(\lambda)q_2(\lambda)$ showing the positioning of the four roots r_i.

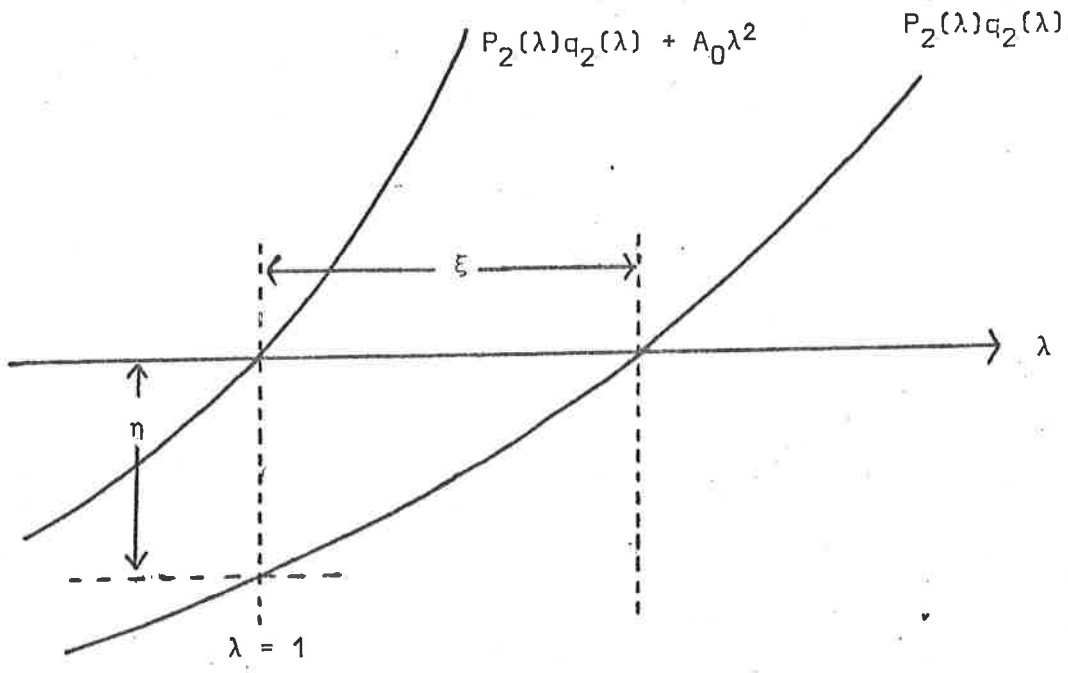

Fig. 9 : Enlargement of Fig. 8 in region λ = 1

$$\text{i.e.} \quad \xi \leq \frac{A_0 - A}{(p_2q_2)'|_{\lambda=1} + 2A} \ .$$

Then

$$r_1 = 1 + \xi < 1 + \frac{A_0 - A}{(p_2q_2)'|_{\lambda=1} + 2A} \ .$$

Using the fact that $p_2(1)q_2(1) + A_0 = 0$ gives

$$A_0 = \frac{-4r^2\Delta t^2\theta}{2F + K^2}\{(2 - \theta)K^2 + 2(1 - \theta)F\} \ .$$

Now with

$$(p_2(\lambda)q_2(\lambda))'|_{\lambda=1} = \frac{4r\Delta t(1 + r\theta A t)}{2F + K^2}\{(3 - \theta)K^2 + (3 + \theta)F\}$$

and

$$A = 4\Delta t^2\{-K_x^2U^2\frac{(2F - K^2)}{(2F + K^2)} + (1 - \theta)r^2\frac{(K^2(1 - \theta) - 2F\theta)}{2F + K^2}\}$$

we deduce that

$$r_1 < 1 + E/G$$

where $E = A_0 - A$

$$= 4\Delta t^2(K_x^2U^2(2F - K^2) - r^2K^2)/(2F + K^2)$$

and

$$G = (p_2q_2)'_{\lambda=1} + 2A$$

$$= \frac{4r\Delta t}{(2F + K^2)}\{(3 - \theta)K^2 + (3 + \theta)F\}$$

$$- 8\Delta t^2K_x^2U^2\left(\frac{2F - K^2}{2F + K^2}\right)$$

$$+ \frac{4\Delta t^2r^2}{2F + K^2}\left(K^2(\theta^2 - \theta + 2) + F(5\theta - 1)\theta\right) \ .$$

The condition $A_0 > A$ requires that $E > 0$, a necessary condition for this being $2F > K^2$. We know, therefore, that as Δt becomes small, $k_x\Delta x$ and $k_y\Delta y$ also become small, k_x and k_y being bounded. Hence

$$G = \frac{4r\Delta t}{2F + K^2}\{(3 - \theta)K^2 + (3 + \theta)F\} + O(\Delta t^2)$$

and $r_1 \leq 1 + E/G$

$$= 1 + \frac{\{K_x^2U^2(2F - K^2) - r^2K^2\}\Delta t}{r\{(3 - \theta)K^2 + (3 + \theta)F\}} + O(\Delta t^2)$$

$$= 1 + O(\Delta t) \quad .$$

The only thing left to show before the demonstration of L - R stability is complete is that the high frequency modes which arise when $k_x\Delta x$ is fixed as $\Delta t \to 0$ are stable. For this we need all the roots of (4.C.1) to be bounded by 1 in modulus in the limit $\Delta t \to 0$; hence

$$(\lambda - 1)^4 + 4\lambda^2\{U\frac{\Delta t}{\Delta x}\sin k_x\Delta x\}^2 = 0$$

must have roots λ_i such that $|\lambda_i| \leq 1$. This is only possible when

$$U\frac{\Delta t}{\Delta x} \leq 1 \quad .$$

(ii) growth rates and position of neutral curve

We now wish to specify regions for which $|\lambda| \leq 1$. The analysis of the position of the roots of (4.C.1) shows that when $A > A_0$ (see previous section) we can say that $|\lambda| \leq 1$, with one root actually at +1 when $A = A_0$. Hence setting $A = A_0$ we find that

$$K_x^2U^2(2F - K^2) = r^2K^2 \quad ,$$

and so there is no growth for the lowest wave number modes given by

$$\frac{K_x^2}{K^2}(2F - K^2) > \frac{r^2}{U^2} \quad . \qquad (4.C.2)$$

To deduce an approximation for C_λ we note that ε is small and that, in general, $r < 1$: hence ignoring terms involving $r\varepsilon$ we find that C_λ almost satisfies

$$C_\lambda^2(K^2 + 2F) + 2C_\lambda(ir(K^2 + F)/K_x) - (r^2K^2/K_x^2 + U^2(K^2 - 2F)) = 0$$

$$\Rightarrow \quad C_\lambda \simeq -\frac{ir}{K_x}\left(\frac{K^2 + F}{K^2 + 2F}\right) \pm i\{U^2(4F^2 - K^4) + r^2F^2/K_x^2\}^{\frac{1}{2}} \Big/ (K^2 + 2F) \quad .$$

Hence when there are growing modes C_λ is entirely imaginary and

$$C_I = Im(C_\lambda) + O(\Delta t^2)$$

$$= -\frac{r}{K_x}\left(\frac{K^2 + F}{K^2 + 2F}\right) + \{U^2(4F^2 - K^4) + r^2F^2/K_x^2\}^{\frac{1}{2}} \Big/ (K^2 + 2F) + O(\Delta t^2) \quad .$$

(4.C.3)

At this point we may also observe that (4.5) gives the following expression for γ^h :

$$\gamma^h = \frac{[K^2(C_\lambda - U) + F(C_\lambda + U)] + i[rK^2/K_x + r\theta\varepsilon(K^2 + F)/K_x]}{F(C_\lambda - U) + iFr\theta\varepsilon/K_x} \quad .$$

(4.C.4)

(iii) positioning of the spurious modes

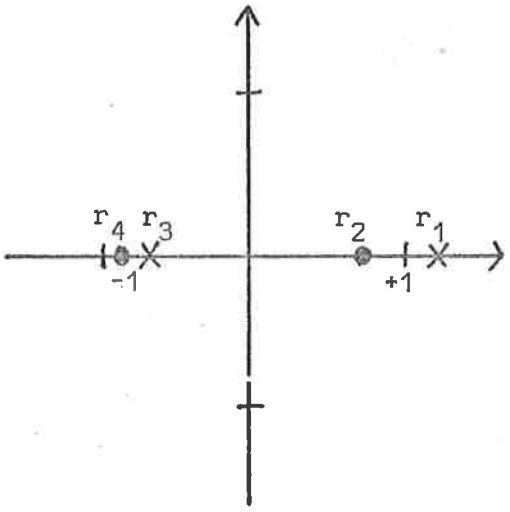

The fastest growing mode is the true mode; it is possible that r_4 (a computational mode) will also grow while r_2 and r_3 both decay. The system is, therefore, relatively stable and no problems with growing spurious modes will be encountered.

5. COMPARISON BETWEEN THE LINEAR BEHAVIOUR OF THE DIFFERENTIAL AND DIFFERENCE SYSTEMS

The main aim of the analysis of the preceding two sections has been to derive complementary results for the behaviour of the differential equation and the difference scheme respectively. The motivation for this was two fold: first to determine how well the differential equation is modelled by the difference scheme for any given resolution (Δx, Δy, Δt) and secondly to provide a yardstick by which the operation of the computer program could be shown to be satisfactory. We shall consider both of these aspects in this section, beginning with a comparison between the two theories for the cases (A), (B) and (C) previously considered.

(A) $r = 0; \beta = 0$

There are three main results to consider here, namely the position of the marginal curve, the growth rate and the phase shift:

Differential equation	Difference scheme
Growth if $k^2 < k_c^2 = 2F$ (3.A.2)	Growth if $K^2 < K_c^2 = 2F$ (4.A.2)
$c_I = U\left(\frac{2F - k^2}{2F + k^2}\right)^{\frac{1}{2}}$ (3.A.3)	$C_I = \frac{K_x}{k_x} U\left(\frac{2F - K^2}{2F + K^2}\right)^{\frac{1}{2}}$ (4.A.3)
$\gamma = \frac{k^2 + F}{F} + \frac{2FU}{F(c - U)}$ (3.A.4)	$\gamma^h = \frac{K^2 + F}{F} + \frac{2FU}{F(C_\lambda - U)}$ (4.A.4)

It is obvious that as $\Delta t \to 0$ for a fixed wave mode, the difference scheme approximates asymptotically the differential equation. The following values of k_c & K_c demonstrate the closeness of the approximation for various wave modes and mesh refinements.

Wave number	k_c	33 x 33 points	65 x 33 points	129 x 129 points
		K_c	K_c	K_c
1	3.2038	3.2024	3.2033	3.2037
2	3.3836	3.3794	3.3803	3.3833
3	3.6637	3.6487	3.6495	3.6628
4	4.0232	3.9825	3.9832	4.0206
6	4.9073	4.7439	4.7445	4.8968

The difference scheme, therefore, always underestimates the position of the neutral curve, but for low wave numbers, e.g. ℓ = 1, 2, 3, a mesh of 33 x 33 points is adequate and a 65 x 33 mesh is little improvement. A table giving numerical comparisons of $k_x c_I$ with $k_x C_I$ for a 33 x 33 mesh is given below (for a 33 x 33 mesh Δx = .3125 = 10 Δy).

F	ℓ = 1		ℓ = 2		ℓ = 3	
	$k_x C_I$	C_I/c_I	$k_x C_I$	C_I/c_I	$k_x C_I$	C_I/c_I
5	-	-	-	-	-	-
6	.03509	.9960	.03854	.9992	-	-
7	.04931	.9945	.07958	.9794	.05470	1.0302
8	.05872	.9940	.10234	.9764	.11158	.9629
9	.06574	.9936	.11854	.9749	.14389	.9530
10	.07127	.9934	.13105	.9739	.16724	.9486

We can see that the numerical growth rate for the first three modes should be better than a 95% approximation to the true linear growth rate for a resolution of 33 x 33 points, and considerably better in the case of wave number 1. The phase shift being of less importance, we quote just one typical value of γ and γ^h for comparison, namely at F = 9 and ℓ = 1:

$\gamma = .57024 - .82148i \Rightarrow \gamma = (1 + 2 \times 10^{-6})e^{(-0.963999i)}$

$\gamma^h = .56973 - .82183i \Rightarrow \gamma^h = (1 - 2 \times 10^{-6})e^{(-0.964618i)}$

Thus there is virtually no error in the amplitude or phase of γ^h.

(B) $\underline{r = 0 \; ; \; \beta \neq 0}$

We again gather together the main results of the linear theory:

Differential Equation	Difference Scheme
Growth if $k^4(4F^2 - k^4) > F^2\beta^2/U^2$ (3.B.2)	Growth if $K^4(4F^2 - K^4) > F^2\beta^2/U^2$ (4.B.2)
$C_I = \frac{\{k^4U^2(4F^2 - k^4) - F^2\beta^2\}^{\frac{1}{2}}}{k^2(k^2 + 2F)}$ (3.B.3)	$C_I = \Gamma\frac{\{k^4U^2(4F^2 - K^4) - F^2\beta^2\}^{\frac{1}{2}}}{K^2(k^2 + 2F)}; \Gamma \sim 1$ (4.B.3)
$\gamma = \frac{k^2(c-U) + \beta + F(c + U)}{F(c-U)}$ (3.B.4)	$\gamma^h = \frac{k^2(C_\lambda - U) + \beta + F(C_\lambda + U)}{F(C_\lambda - U)}$ (4.B.4)

For $F = 10$, $\beta = 1$, $U = .2$ the modes for which $k^4 \epsilon [6.35, 393.65] = I$ are unstable whereas on the finite difference mesh only the modes for which $K^4 \epsilon I$ are unstable. Since for any mesh and wave mode $K^4 < k^4$, this means that we are overestimating the size of the unstable domain.

For $F = 7$, $\beta = 12$, $U = .2$ with wave number 2, $C_I/c_I = .978$ on a 33 x 33 mesh. So we are estimating c_I to within about 2%: for smaller values of β we do better since Γ is nearer 1 in (4.B.3).

For the same parameters γ and γ^h are found to be

$\gamma = -.48063 - .98666i \Rightarrow \gamma = 1.0975e^{-2.02409i}$

with $\gamma^h = -.48121 - .99153i \Rightarrow \gamma^h = 1.10213e^{-2.02263i}$

which means $|\gamma|/|\gamma^h| = 1.004$ and the phase shift $= 0.05^o$.

(C) $r \neq 0$; $\beta = 0$

This is, perhaps, the most interesting case to look at; however, to complete a table of comparisons we must make an approximation to $C_I = I_m(C_\lambda)$ since λ is now the root of a quartic with non-zero coefficients for λ^3 and λ. The table is as follows:-

Differential Equation	Difference Scheme
Growth iff $\frac{k_x^2}{k^2}(2F-k^2) > \frac{r^2}{U^2}$ (3.C.2)	Growth iff $\frac{K_x^2}{K^2}(2F-K^2) > \frac{r^2}{U^2}$ (4.C.2)
$c_I = \frac{-r}{k_x}\left(\frac{k^2+F}{k^2+2F}\right) + \frac{(U^2(4F^2-k^4)+F^2r^2/k_x^2)^{\frac{1}{2}}}{(k^2+2F)}$ (3.C.3)	$C_I \approx -\frac{r}{K_x}\left(\frac{K^2+F}{K^2+2F}\right) + \frac{(U^2(4F^2-K^4)+r^2F^2/K_x^2)^{\frac{1}{2}}}{(K^2+2F)}$ (4.C.3)
$\gamma = \frac{k^2+F}{F} + \frac{2FU}{F(c-U)} + \frac{irk^2/k_x}{F(c-U)}$ (3.C.4)	$\gamma^h \approx \frac{K^2+F}{F} + \frac{2FU}{F(C_\lambda-U)} + \frac{irk^2/K_x}{F(C_\lambda-U)}$ (4.C.4)

The graphs below show the neutral curves for wave numbers 1 to 4 in the (F, r) plane, the regions of instability for each wave mode being above its neutral curve.

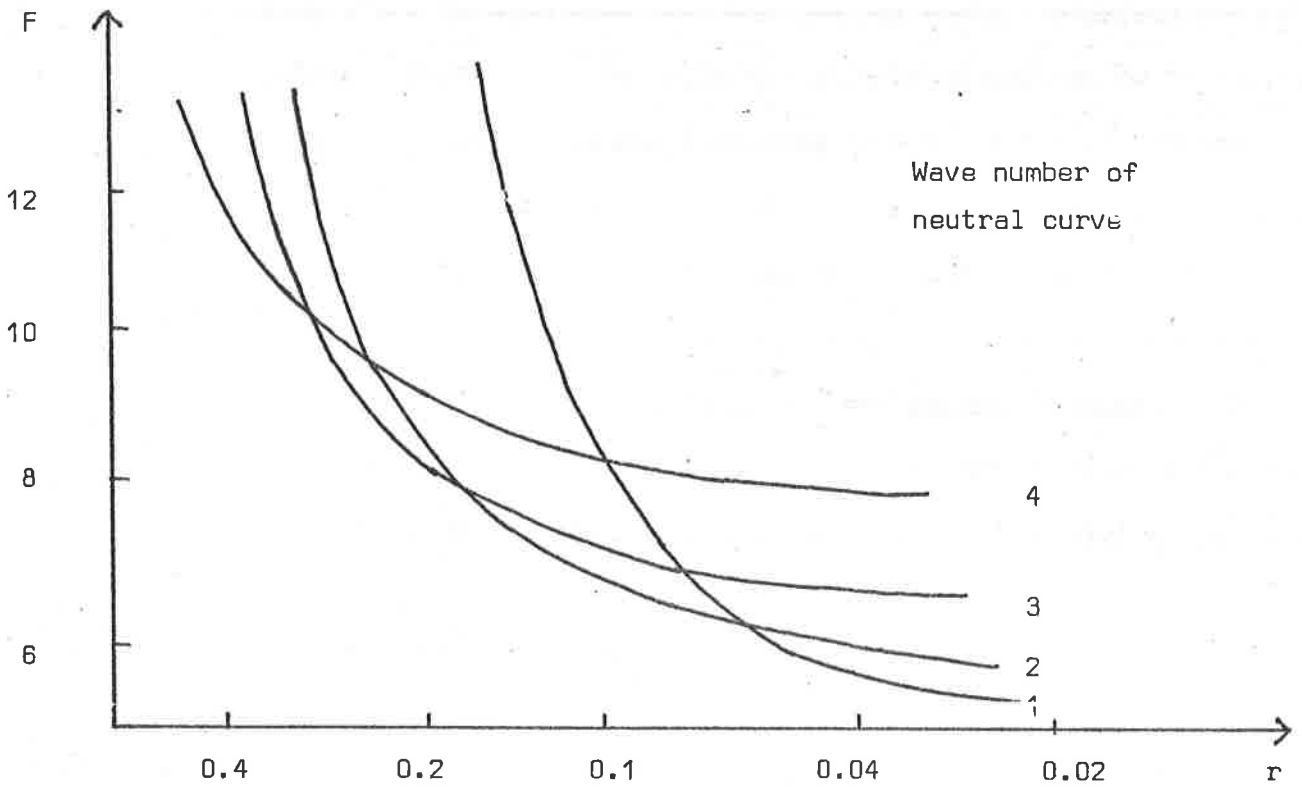

Computation of the roots of the quartic (4.C.1) gives the following table comparing $k_x c_I$ with $k_x C_I$, the ratio C_I/c_I being given:

Wave number	F \ r	0.2	0.1
1	7	-	-
	8	-	-
	9	-	.9346
	10	-	.9690
	11	-	.9762
2	7	-	.8769
	8	-	.9387
	9	-	.9483
	10	.7098	.9520
	11	.8609	.9540
3	7	-	-
	8	-	.9103
	9	.5407	.9155
	10	.8057	.9175
	11	.8498	.9183

(for a 33 x 33 mesh)

This table shows us that away from the marginal curve the approximation is quite good but near the marginal curve we may well need to use a finer mesh, especially for the higher wave numbers and larger values of r. Typical values of F and r give the following values for γ and γ^h : (F = 7, r =.1, U = .2)

γ = .67010 - .74227i => $\gamma = e^{-.8365i}$

γ^h = .66291 - .74870i => $\gamma^h = e^{-.8461i}$

which represents a phase shift error of less than 0.5^o.

It is fair to conclude from the results of (A), (B) and (C) above that a mesh of 33 x 33 points should yield an approximation to the differential equation which is not only qualitatively correct, but which, in the majority of cases, is also accurate to within 10% and usually to within 5%. We now give results of a computer program written to implement the algorithm, to check both the analysis and the program.

(i) Testing for growth if $K^2 < K_c^2 = 2F$ when $r = \beta = 0$.

A series of five runs was performed for values of F just less than and just greater than $\frac{1}{2}K_c^2$, the critical value. A mesh of 33 x 33 points was used along with wave no. 2. For these parameters $\frac{1}{2}K_c^2 = 5.71031$ compared with $\frac{1}{2}k_c^2 = 5.72437$. The values of F used were 5.71000 incremented in steps of 0.0001, the first four being subcritical on the linear theory for the difference scheme, all five being subcritical on the linear theory for the differential equations.

The observations were in complete accord with the theory outlined above for the subcritical computations all exhibited decaying modes whereas the supercritical run exhibited growth. In fact a sequence of runs conducted with $F \in (5.71030, 5.71040)$ also agreed with theory.

To check the method with a higher wave mode a series of runs around $\frac{1}{2}K_c^2 = 7.93006$ (with wave number 4) was conducted, and gave the expected results.

(ii) Testing for growth if $K_x^2(2F - K^2)/K^2 > r^2/U^2, \beta = 0$.

Now we include the dissipative mechanism of Ekman suction and pumping on the top and bottom layers and test the program around the point F = 6.6623, r = .1, with wave mode 2 and U = .2. A series of five runs with F = 6.64 incremented by 0.05 was carried out with the desired result that the first three exhibited decay (i.e. were subcritical) and the last two showed exponential growth.

(iii) Testing the growth rate for $r \neq 0$, $\beta = 0$.

This was tested for wave mode 2 and wave mode 3 in the regions $F = 7$, $r = .1$ and $F = 9$, $r = .2$. Two tables showing the growth rates predicted for the differential equation, the predicted growth rates for the difference scheme and those observed in the model are given: (mesh = 33 x 33 points).

($r = .1$)

F	$k_x c_I$	$k_x C_I$	Observed
6.9	875	740	728
7.0	1170	1026	1014
7.1	1453	1300	1289

($r = .2$)

F	$k_x c_I$	$k_x C_I$	Observed
9.1	1498	921	899
9.2	1773	1178	1156
9.3	2042	1428	1407
9.4	2302	1672	1650

For these computations the starting conditions were such that

$$\Phi_2^0 = \gamma^h \Phi_1^0$$

so that the model would not have to adjust the relative phases of Φ_2 and Φ_1 before growth would begin. The results seem to be entirely satisfactory.

6. NONLINEAR THEORY AND RESULTS

The only way in which non-linear behaviour has been investigated theoretically is through asymptotic expansion methods. Pedlosky has conducted theoretical analyses in several different portions of parameter space and has derived some interesting results. However, his theory is restricted to weak non-linearities, i.e. to regions near the neutral curve, and to flows with an oversimplified modal structure.

We first summarise these non-linear results without giving the details of their derivation. In the expansions the lowest order solution is the linear solution derived in Section III, with a slowly varying amplitude $A(t)$. Then the second order solution is a mean-flow correction term arising out of the self-interaction of the main wave (the linear solution), and is therefore independent of x. At the third order solution secularities will occur unless $A(t)$ satisfies a particular non-linear ODE; making such a requirement on $A(t)$ renders a finite amplitude steady solution for the main wave provided r is sufficiently large. For smaller values of r a vacillation in the wave amplitude $A(t)$ has been shown to occur.

At the present time we are concerned with the steady-state equilibration phenomenon since for these solutions quantitative comparisons between theory and the numerical model are altogether easier than those for the vacillating solutions.

It should be pointed out that the results obtainable from an analysis of the differential equation are, in principle, obtainable from a similar analysis of the difference scheme. A treatment of the difference scheme in the case $r \neq 0$, $\beta = 0$ rendered the same

mean-flow correction as that for the differential equations, but with the coefficients arising from differential operators replaced by their discrete analogues.

Some non-linear numerical results are now reviewed. First of all, for non-linear equilibration, we have drawn up two tables to show equilibration amplitudes for runs in two different parts of parameter space, and for different wave numbers. Both were computed on 33 x 33 meshes.

(r = .1)

F	Calculated from analysis	Observed in model
6.9	176	169
7.0	202	200
7.1	225	226

(wave mode 2)

(r = .2)

F	Calculated from analysis	Observed in model
9.0	184	142
9.1	203	170
9.2	220	192
9.3	235	211

(wave mode 3)

Caution should be exercised in the interpretation of the results for wave mode 3, for these results may be near the limit for which the weakly non-linear theory is strictly applicable. Boville (1980) has also observed that under similar conditions a spectral model of the same set of equations can overestimate the weakly nonlinear amplitude.

The other important feature that the weakly nonlinear theory gives is the amplitude of the meanflow correction. Theory for the point (F, r) = (6.0, 0.04) gives the meanflow correction.

$$69 \cos \pi y - 4.6 \cos 3\pi y + \text{higher frequency terms}$$

whereas in the numerical model it is

$$70 \cos \pi y - 4.2 \cos 3\pi y + \text{higher frequency terms.}$$

An example of a nonlinear equilibration in which the GHOST (the Graphical Output System) suite of subroutines (implemented on a CDC 7600) is used to produce computer plotted graphs is presented below in Fig. 10.

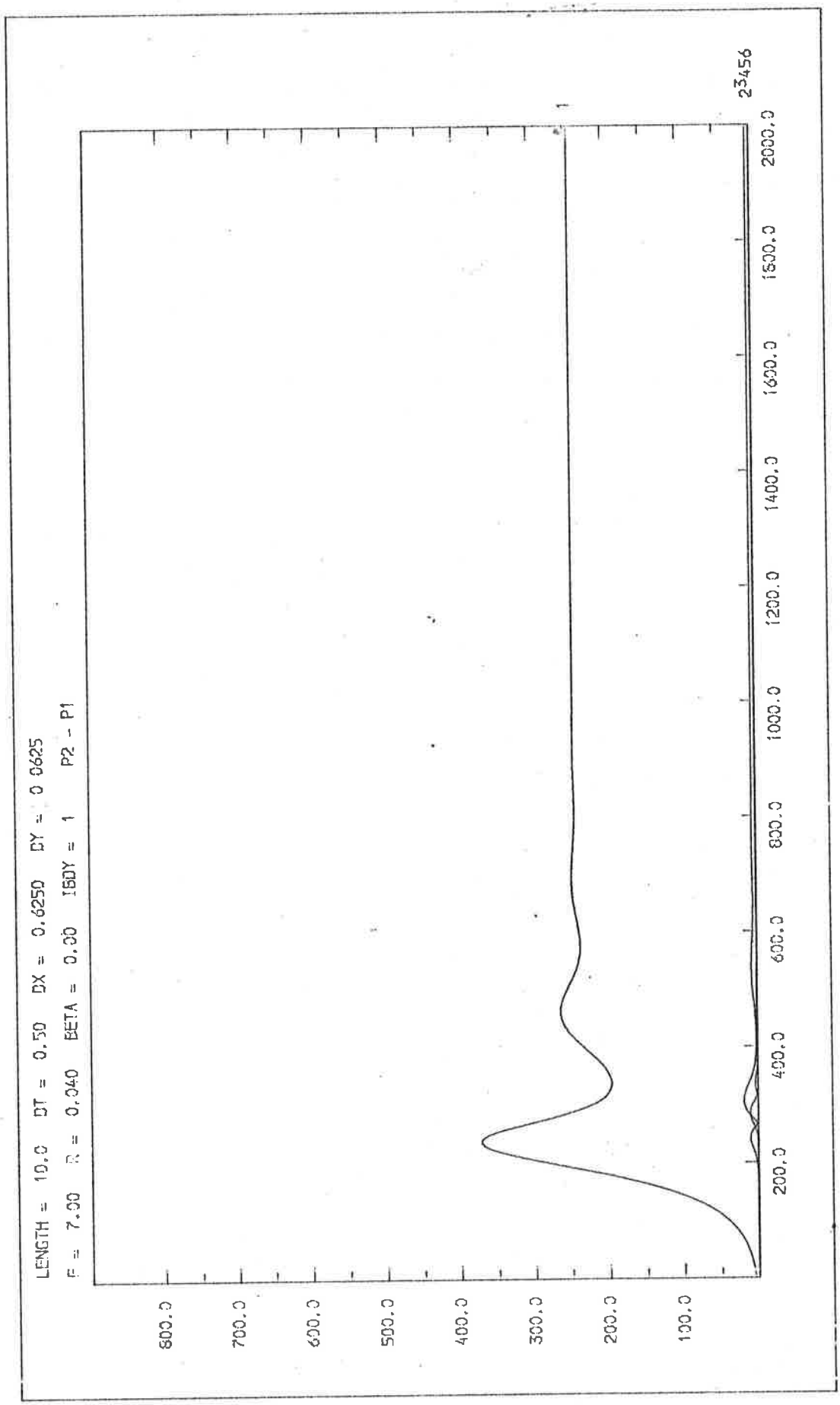

Fig. 10 : Wave amplitudes of $\psi_2 - \psi_1$ during a typical computation.
Wave mode 1 is the main wave, with harmonic mode no. 3

7. CONCLUSION

The verification of the algorithm and the program has been the motivation of this report. We have sought to present a comparison of the linear behaviour of the differential equations with that of the algorithm for various different parameter regimes, and to demonstrate the correct operation of the computer program. This has been done for the cases when both r and β are zero, and when either r or β is non-zero, by showing that the linearised algorithm accurately approximates the linearised differential system with the coefficients arising from differential operators replaced by those arising from the corresponding discrete operators.

In particular, we are able to show that by using leapfrog time-differencing an algorithm is produced which approximates well the regions of growing modes and decaying modes.

We have also clearly demonstrated that linear growth rates have been well reproduced in the algorithm; such a feature is important in the applications planned for the model (see below). The last useful result from the linear analysis is that the phase shift between modes in the two layers is well approximated by the algorithm. Indeed, in many subsequent computations we have observed that $|\gamma^h| = 1$ throughout which indeed increases confidence in the model.

One feature of the algorithm which should be noted is that leapfrog differencing ensures an absence of dissipation for the linear problem and that the Arakawa nonlinear formulation ensures conservation of energy and enstrophy within the accuracy of the time-stepping. When the energetics in the system are worked through, it is clear that the dissipative Ekman terms act as the sources and sinks of energy, and experiment has shown that the level of dissipation greatly affects the type of finite amplitude solution derived. It is therefore important

to ensure that no additional sources or sinks are created, thereby upsetting the energy balance within the model.

Numerical experiments with the model both at small (i.e. linear theory level) and at finite amplitude appear to indicate the correct and satisfactory operation of the program. The stability/instability criterion of linear theory was found to be highly accurate and any doubt concerning growth rates can be dispelled by observing that as the mainwave grows, energy passes to higher frequency modes, by self-interaction and interaction with the mean-flow correction, thereby slightly reducing the growth rate. For the finite amplitude results, although these are rather limited, agreement seems to be adequate in view of the weaknesses outlined in the nonlinear theory.

Now that confidence in the correct operation of the algorithm and model has been established, a series of experiments can begin with the intention of understanding more fully the finite amplitude dynamics of baroclinic waves. Particular emphasis will be made on using the model in strongly nonlinear regions of parameter space where no analytic theory can be developed, and where regular vacillations should be observed.

Other application areas include the addition of more physics in the model. The insertion of Ekman layers at the interface or indeed the effects of surface tension at the interface seem to be the two most important aspects of the physics which are currently missing. When surveying possible uses for the model it is important to include aspects for which a finite difference model is particularly well suited. The most obvious area in which the finite difference model can operate where a spectral model, for example, cannot, is for flow over a topography with sharp corners.

Our intention will be to increase our understanding in the areas outlined above while paying particular attention to effects of mesh resolution and to the influence on wave interactions of using various

orders of nonlinear differencing.

APPENDIX 1 : THE EKMAN LAYERS

If a fluid is in geostrophic balance, then since u_n and v_n are z independent, boundary layers must exist at the solid horizontal boundaries whenever they have a velocity different from that in the mean flow. In the two layer system we have, to first order, geostrophic balance, and hence the presence of Ekman layers at the bottom and top of the channel on the boundaries z = 0 and 1.

When we look back to the non-dimensional Navier-Stokes equations we find that near z = 0 say, for the viscous terms to balance the Coriolis forces we need

$$E\, u_{zz} = 0\ (1)$$

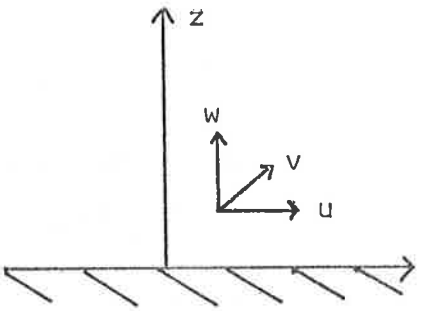

Since u and v are 0 (1) and E << 1 this means that we require a vertical scale of variation

$$\Delta = E^{\frac{1}{2}} = \frac{1}{D}\left(\frac{2\upsilon}{fo}\right)^{\frac{1}{2}}.$$

This layer, whose width is independent of the relative motion of the fluid, is called an Ekman boundary layer and has dimensional thickness of $(2\nu/fo)^{\frac{1}{2}}$.

Near z = 0, within the Ekman layer, we represent the velocity fields in the following way:

$$u = u_B\,(x, y, \eta, \varepsilon, E) = u_B^{(0)}\,(x, y, \eta) +$$

$$v = v_B\,(x, y, \eta, \varepsilon, E) = v_B^{(0)}\,(x, y, \eta) +$$

$$w = w_B\,(x, y, \eta, \varepsilon, E) = 0 + E^{\frac{1}{2}} w_B^{(1)}\,(x, y, \eta) +$$

where $\eta = z/E^{\frac{1}{2}}$ is the natural co-ordinate scaling in the boundary layer, and the subscript B denotes a boundary layer quantity. Substituting these into the non-dimensional Navier-Stokes equations yields:

$$-v_B^{(0)} = \frac{-\partial p_B^{(0)}}{\partial x} + \tfrac{1}{2}\frac{\partial^2 u_B^{(0)}}{\partial \eta^2}$$

$$u_B^{(0)} = \frac{-\partial p_B^{(0)}}{\partial y} + \tfrac{1}{2}\frac{\partial^2 v_B^{(0)}}{\partial \eta^2}$$

$$0 = \frac{-\partial p_B^{(0)}}{\partial z}$$

with $$\frac{\partial u_B^{(0)}}{\partial x} + \frac{\partial v_B^{(0)}}{\partial y} = \frac{-\partial w_B^{(1)}}{\partial \eta}$$

Solving these equations with the conditions:

$$u_B^{(0)} = 0$$

and $$v_B^{(0)} = 0$$

on $\eta = 0$, gives the result that

$$w_B^{(1)} = -\tfrac{1}{2}\zeta_I^{(0)}\{1 - \sqrt{2}\exp(-z/E^{\frac{1}{2}})\sin(z/E^{\frac{1}{2}} + \pi/4)\},$$

where the subscript I denotes a quantity of the interior flow. Now applying matching conditions at the edge of the boundary layer gives

$$w_I(x, y, 0) = E^{\frac{1}{2}} w_B^{(1)}(x, y, \infty)$$
$$= \tfrac{1}{2}E^{\frac{1}{2}}\zeta_I^{(0)}$$

similarly for the surface $z = 1$ we find

$$w_I(x, y, 1) = -\tfrac{1}{2}E^{\frac{1}{2}}\zeta_I^{(0)}$$

Applying these conclusions to our particular problem we find

that $$w_1^{(1)}(x, y, 0) = \frac{1}{\varepsilon} w_1(x, y, 0) = \tfrac{1}{2}\frac{E^{\frac{1}{2}}}{\varepsilon}\zeta_1^{(0)}$$

and $$w_1^{(1)}(x, y, 1) = \frac{1}{\varepsilon} w_2(x, y, 1) = -\tfrac{1}{2}\frac{E^{\frac{1}{2}}}{\varepsilon}\zeta_2^{(0)}$$

APPENDIX 2 : THE CONSISTENCY CONDITIONS

There is a consistency condition arising from the Poisson equation derived in the numerical treatment of the two-layer system, and another one, similar to that for the Poisson equation, arising from the Helmholtz equation. Suppose we want to solve the equations in $\Omega = [0, L_x] \times [0,1]$.

Let $\phi_s = \phi_1 + \phi_2$, $q_s = q_1 + q_2$. Then

$$\int_\Omega \nabla^2 \phi_s = \int_\Omega q_s = Q, \text{ say.}$$

But $\int_\Omega \nabla^2 \phi_s = \left[\int_0^{L_x} \frac{\partial \phi_s}{\partial y}\, dx\right]_{y=0}^{y=1}$, because of the periodicity condition $\phi_s(x) = \phi_s(x + L_x)$. The boundary conditions imposed on ϕ_s are

$$\frac{\partial \phi_s}{\partial x} = 0, \quad \frac{\partial}{\partial t} \int_0^{L_x} \frac{\partial \phi_s}{\partial y}\, dx = 0, \quad \text{for } y = 0, 1$$

or $$\int_0^{L_x} \frac{\partial \phi_s}{\partial y}\, dx = I_0, I_1 \quad \text{(constant in time) for } y = 0, 1$$

Thus we must have $Q = I_1 - I_0$, and so Q is constant in time. Now

$$\frac{dQ}{dt} = \int_\Omega \frac{\partial q_s}{\partial t} = -r \int_\Omega \nabla^2 \phi_s - \beta \int_\Omega \frac{\partial \phi_s}{\partial x} - \int_\Omega J_1 - \int_\Omega J_2$$

where $J_1 = J(\phi_1, q_1)$, $J_2 = J(\phi_2, q_2)$.

Therefore $\frac{dQ}{dt} = -r\, Q - \beta \left[\int_0^1 \phi_s dy\right]_{x=0}^{x=L_x} - \int_\Omega J_1 - \int_\Omega J_2$.

But $$\int_\Omega J_1 = \int_\Omega \frac{\partial \phi_1}{\partial x} \frac{\partial q_1}{\partial y} - \frac{\partial \phi_1}{\partial y} \frac{\partial q_1}{\partial x}$$

$$= \int_\Omega \frac{\partial}{\partial x}\left(\phi_1 \frac{\partial q_1}{\partial y}\right) - \frac{\partial}{\partial y}\left(\phi_1 \frac{\partial q_1}{\partial x}\right)$$

$$= \left[\int_0^1 \phi_1 \frac{\partial q_1}{\partial y}\, dy\right]_{x=0}^{x=L_x} - \left[\int_0^{L_x} \phi_1 \frac{\partial q}{\partial x}\, dx\right]_{y=0}^{y=1}$$

$$= \left[\phi_1 q_1\right]_{x=0}^{x=1} {}_{y=0}^{y=1} + \left[\int_0^{L_x} \frac{\partial \phi_1}{\partial x} q_1\, dx\right]_{y=0}^{y=1}$$

$$= 0$$

Similarly for $\int_\Omega J_2$.

Therefore

$$-rQ = \frac{dQ}{dt} = 0 \quad \text{since Q constant in time}$$

and so $\left[\int_0^L x \frac{\partial \phi_s}{\partial y}\, dx\right]_{y=0}^{y=1} = 0$ is a necessary consistency condition.

In a similar manner denoting $\phi_1 - \phi_2$ by ϕ_D we find

$$\left[\int_0^L x \frac{\partial \phi_D}{\partial y}\, dx\right]_{y=0}^{y=1} = 0$$

arises from the Helmholtz problem. Combining these two together we show that

$$\int_\Omega \nabla^2 \psi_1 = \int_\Omega \zeta_1 = 0 \qquad \forall t$$

and

$$\int_\Omega \nabla^2 \psi_2 = \int_\Omega \zeta_2 = 0 \qquad \forall t$$

or equivalently,

$$\left[\int_0^L x \frac{\partial \psi_1}{\partial y}\, dx\right]_{y=0}^{y=1} = 0 \qquad \forall t$$

and

$$\left[\int_0^L x \frac{\partial \psi_2}{\partial y}\, dx\right]_{y=0}^{y=1} = 0 \qquad \forall t$$

APPENDIX 3 : THE FACR ALGORITHM USED IN POT 1

The problem which we are concerned with is highly amenable to treatment by a Rapid Elliptic Solver using Fourier Analysis and Cyclic Reduction. The procedure employed in the program POT 1 is, in fact, the FACR(ℓ) algorithm with $\ell = 1$. The parameter ℓ indicates the number of levels of cyclic reduction that are performed before Fourier analysis takes place. As ℓ varies from 0 to $\log_2 n$ (where n is the number of intervals in the grid) we have a range of algorithms varying from a basic method involving no cyclic reduction to the Buneman algorithm involving no Fourier analysis. Of particular importance is the existence of an optimum value of $\ell \simeq \log_2 (\log_2 n)$, which leads to an algorithm with a minimum operation count proportional to $n^2 \log_2 (\log_2 n)$.

Basic Method

We want to solve $(\nabla^2 - \lambda^2)\, \phi = s$

on a rectangular region with Dirichlet conditions along one boundary and periodic conditions along the other. For a square mesh, the usual five point difference formula for ∇^2 yields

$$\underline{\phi}_{j-1} + A\underline{\phi}_j + \underline{\phi}_{j+1} = \underline{S}_j$$

where $\underline{\phi}_j$ is the potential along the line $y = jh$, h being the mesh size and

$$A = \begin{bmatrix} -4-\lambda^2h^2 & +1 & & 0 \\ +1 & & \ddots & \\ & \ddots & & +1 \\ 0 & & +1 & -4-\lambda^2h \end{bmatrix}$$

We then perform one cyclic reduction, for FACR(1), eliminating all the odd rows, and retaining only the even ones. This gives

$$\underline{\phi}_{j-2} + (2I - A^2)\, \underline{\phi}_j + \underline{\phi}_{j+2} = \underline{S}_{j-1} - A\underline{S}_j + \underline{S}_{j+1}$$

where j is even.

We can then perform Fourier analysis using the discrete transforms to obtain

$$\hat{\phi}^k_{j-2} + \alpha_R \hat{\phi}^k_j + \hat{\phi}^k_{j+2} = \hat{S}^k_j \qquad \text{for } k = 1, \ldots, n-1$$

where $\alpha_k = 2 - \left(4 + \lambda^2 h^2 - 2 \cos \frac{k\pi}{n}\right)^2$

These systems are then solved by cyclic reduction or Gauss elimination for each $\hat{\phi}^k_j$. Fourier synthesis then returns values of $\underline{\phi}_j$ on the even lines and we know that

$$A\underline{\phi}_{j-1} = \underline{S}_{j-1} - \underline{\phi}_{j-2} - \underline{\phi}_j \qquad (j \text{ even})$$

Cyclic reduction or Gaussian Elimination here provides values for $\underline{\phi}_j$ on every line, and the problem is solved. Hockney (1970) has given a formula for the number of operations in the FACR/ℓ) algorithm as a function of the number of levels of reduction and assuming that scalar cyclic reduction is used for the solution of the tridiagonal systems,

$$T(\ell) = n^2[4.5\ell + 3 + (5 \log_2 n - 4)2^{-\ell}]$$
(FACR)

Differentiation gives ℓ^*, the optimum choice of ℓ, as $\log_2(\log_2 n)$ with

$T^*_{FACR} \simeq 4.5\, n^2 \log_2(\log_2 n)$.

Hence for computation on a 32 x 32 grid, where $n = 2^5$, $\ell^* = 1$ and $T^* = 19$ operations per mesh point. This is equivalent to a large number of iterations using SOR.

References

1. ARAKAWA, A. (1966), Computational design for long-term integrations of the equations of fluid motions. Part 1 : 2-D flows. J. Comp. Phys.; 1, 119.
2. BOVILLE, B.A. (1980), Amplitude vacillation on an f-plane. J. Atmos. Sci., 37, 1413.
3. DRAZIN, P.G. (1970), Non-linear baroclinic instability of a continuous zonal flow. Q.J. Royal Met. Soc., 96, 667.
4. GILL, A.E. GREEN, J.S.A. and SIMMONS, A.J. (1974), Energy partition in the large scale ocean circulation and the production of mid-ocean eddies. Deep Sea Res., 21, 499.
5. HART, J.E. (1972), A laboratory study of baroclinic instability. Geophys. Fluid Dyn., 3,181.
6. HIDE, R. (1969), Some laboratory experiments on free thermal convection in a rotating fluid subject to a horizontal temperature gradient and their relation to the theory of the global atmospheric circulation. In the Global Circulation of the Atmosphere ed Corby, Royal Met. Soc., pp 196-221.
7. HIDE, R. and MASON, P.G. (1975), Sloping convection in a rotating fluid. Adv. in Phys., 24, 47.
8. HOCKNEY, R.W. (1970), The potential calculation and some applications. Methods in Comp. Phys., 9, 135.
9. HOCKNEY, R.W. (1978), Rapid Elliptic Solvers. Report, Dept. Computer Science, Reading.
10. HOSKINS, B.J. and SIMMONS, A.J. (1976), Baroclinic instability on the sphere: normal modes of the primitive and quasigeostrophic equations. J. Atmos. Sci., 33, 1454.
11. HOSKINS, B.J. and SIMMONS, A.J. (1977), Baroclinic instability on the sphere: solutions with a more realistic tropopause. J. Atmos, Sci., 34, 581.
12. LORENZ, E.N. (1967), The nature and theory of the general circulation of the atmopshere. W.M.O. publication no. 218.
13. PEDLOSKY, J. (1970), Finite amplitude baroclinic waves. J. Atmos. Sci., 27, 15.
14. PEDLOSKY, J. (1971), Finite amplitude baroclinic waves with small dissipation. J. Atmos. Sci., 28, 587.
15. PEDLOSKY, J. (1972), Limit cycles and unstable baroclinic waves. J. Atmos. Sci., 29, 53.

16. PHILLIPS, N.A. (1956), The general circulation of the atmosphere: a numerical experiment. Q.J. Royal Met. Soc., 82, 123.

17. ROACHE, P.J. (1972), Computational Fluid Dynamics. Hermosa Publications.

18. SMITH, R.K. and REILLY, J.M. (1977), On a theory of amplitude vacillation in baroclinic waves : some numerical solutions. J. Atmos. Sci., 34, 1256.